D-A143 003 A NEW APPROACH TO THE EVALUATION OF THE EFFECTS OF 1/2
STRESS STATE AND INTER.. (U) SOUTHWEST RESEARCH INST SAN
ANTONIO TEX DEPT OF MATERIALS SCI.. J E HACK ET AL.
UNCLASSIFIED 31 MAY 84 ARO-17207.3-MS DAAG29-81-K-0049 F/G 11/4 NL

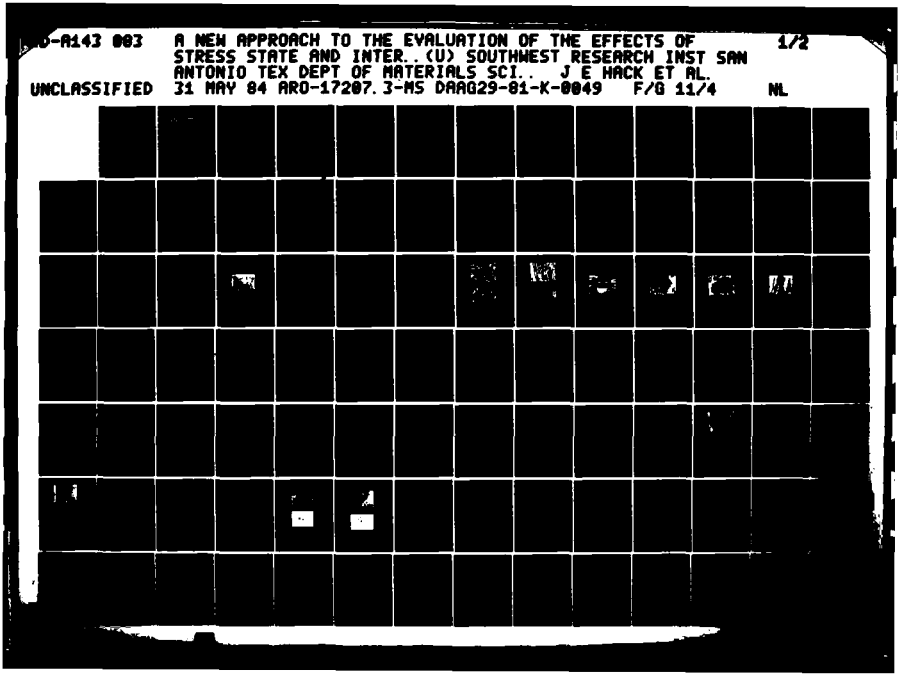

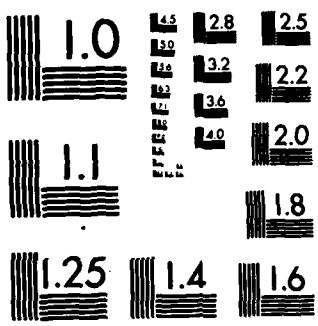

ARO 17207.3-MS

(2)

A New Approach to the Evaluation of the Effects of Stress State and Interfacial Properties on the Behavior of Advanced Metal Matrix Composites

by
J. E. Hack
R. A. Page
G. R. Leverant

TECHNICAL REPORT
Contract No. DAAG29-81-K-0049

for
U.S. Army Research Office
Post Office Box 12211
Research Triangle Park, NC 27709

May 31, 1984

SOUTHWEST RESEARCH INSTITUTE
SAN ANTONIO HOUSTON

SOUTHWEST RESEARCH INSTITUTE
Post Office Drawer 28510, 6220 Culebra Road
San Antonio, Texas 78284

A New Approach to the Evaluation of the Effects of Stress State and Interfacial Properties on the Behavior of Advanced Metal Matrix Composites

by
J. E. Hack
R. A. Page
G. R. Leverant

TECHNICAL REPORT
Contract No. DAAG29-81-K-0049

for
U.S. Army Research Office
Post Office Box 12211
Research Triangle Park, NC 27709

May 31, 1984

Approved:

U. S. Lindholm, Director
Department of Materials Sciences

UNCLASSIFIED
SECURITY CLASSIFICATION OF THIS PAGE (When Data Entered)

AD-A143083

REPORT DOCUMENTATION PAGE		READ INSTRUCTIONS BEFORE COMPLETING FORM
1. REPORT NUMBER	2. GOVT ACCESSION NO. N/A	3. RECIPIENT'S CATALOG NUMBER N/A
4. TITLE (and Subtitle) A New Approach to the Evaluation of the Effects of Stress State and Interfacial Properties on the Behavior of Advanced Metal Matrix Composites		5. TYPE OF REPORT & PERIOD COVERED Technical Report July 1981 - May 1984
		6. PERFORMING ORG. REPORT NUMBER
7. AUTHOR(s) J. E. Hack, R. A. Page and G. R. Leverant		8. CONTRACT OR GRANT NUMBER(s) DAAG29-81-K-0049
9. PERFORMING ORGANIZATION NAME AND ADDRESS Southwest Research Institute Department of Materials Sciences 6220 Culebra Road, P.O. Drawer 28510 San Antonio, TX 78284		10. PROGRAM ELEMENT, PROJECT, TASK AREA & WORK UNIT NUMBERS
11. CONTROLLING OFFICE NAME AND ADDRESS U. S. Army Research Office Post Office Box 12211 Research Triangle Park, NC 27709		12. REPORT DATE May 31, 1984
		13. NUMBER OF PAGES
14. MONITORING AGENCY NAME & ADDRESS(if different from Controlling Office)		15. SECURITY CLASS. (of this report) Unclassified
		15a. DECLASSIFICATION/DOWNGRADING SCHEDULE

16. DISTRIBUTION STATEMENT (of this Report)

Approved for public release; distribution unlimited.

17. DISTRIBUTION STATEMENT (of the abstract entered in Block 20, if different from Report)

NA

18. SUPPLEMENTARY NOTES

The view, opinions, and/or findings contained in this report are those of the author(s) and should not be construed as an official Department of the Army position, policy, or decision, unless so designated by other documentation.

19. KEY WORDS (Continue on reverse side if necessary and identify by block number)

Metal Matrix Composite	Tensile Behavior	Thermal Exposure
Al_2O_3 Fiber	Fatigue	Processing
Magnesium Alloys	Cyclic Cleavage	Defects
Tensile Behavior	Fracture Toughness	

20. ABSTRACT (Continue on reverse side if necessary and identify by block number)

The effects of fiber fraction, fiber orientation and matrix alloy additions on tensile and fatigue behavior were studied in commercially pure magnesium and ZE41A (Mg-4.25Zn-0.5Zr-1.25RE) that were both reinforced with FP alumina fibers. In general, axial properties were found to be dependent on fiber fraction while off-axis properties were not. Off-axis loading resulted in substantial reductions in tensile and fatigue strength in the commercially pure matrix material. Although failure in tensile overload occurred along the weak fiber/matrix interface in off-axis specimens, subcritical fatigue

DD FORM 1 JAN 73 1473 EDITION OF 1 NOV 65 IS OBSOLETE

UNCLASSIFIED
SECURITY CLASSIFICATION OF THIS PAGE (When Data Entered)

FOREWORD

The research reported herein was conducted by Southwest Research Institute, San Antonio, Texas, under Contract DAAG29-81-K-0049. The report summarizes work accomplished during the period July 1981 through May 1984. Drs. John Hurt, John Bailey, and Iqbal Ahmad were the ARO Program Managers. The work was conducted under the general supervision of Dr. Gerald R. Leverant, SwRI Project Manager, with assistance from Mr. John E. Hack and Dr. Richard A. Page. Special acknowledgement is due Drs. Robert Sherman and Kwai S. Chan who assisted with the Auger electron spectroscopy and fracture mechanics analysis, respectively. The technical support of Messrs. Harold Saldana, Kyle Short and Victor Aaron are also greatly appreciated.

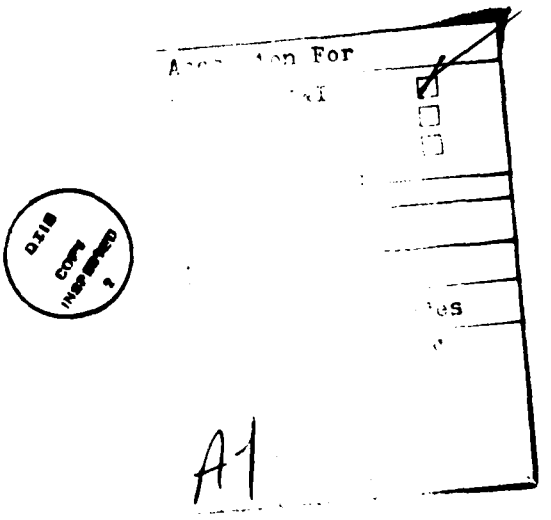

SUMMARY

The reinforcement of metal matrices with high strength and high modulus synthetic fibers to produce a hybrid material possessing attractive structural properties is not a new concept. The combination of recently developed high strength and modulus ceramic fibers with lightweight, ductile metal matrices (principally magnesium and aluminum) has spurred renewed interest in the potential of these materials for applications requiring high specific strength and stiffness, toughness, and fatigue resistance. Implementation of advanced metal matrix composite materials in structural applications has always suffered, however, due to a lack of a quantitative relationship between microstructure and mechanical behavior.

Although a greal deal of work has been performed on fracture mechanisms in metal matrix composites, the results to date have been quite contradictory in nature. The inconsistencies arise from the complex interaction of the fiber/matrix interfacial region with various applied states of stress. In addition, the presence of the fiber/matrix interface in these composites introduces several mechanisms of crack propagation in addition to those observed in monolithic materials. Also, standard metallurgical techniques for modifying the properties of the matrix material (i.e., alloying, heat treatment, deformation processing, etc.) affect the metallurgical structure and properties of the interfacial region as well. Thus, the effects of processing variables on composite behavior through microstructural changes in the matrix are difficult to separate from the effects of those variables on the fiber/matrix interface.

This report summarizes the results of a program which was initiated to overcome these difficulties by developing quantitative relationships between matrix microstructure, composition and properties, fiber orientation and volume percent, and fatigue crack growth behavior in these materials through direct observations of the effects of these variables on the strain field at the tip of a growing crack. The overall program is aimed at

determining the local sequence of events at the tip of a fatigue crack (i.e., matrix failure vs. fiber failure vs. interfacial decohesion) and the critical strain accumulation required for these events to occur. However, very little data exist on the relationships between microstructure and crack growth resistance in metal matrix composites. Thus, the efforts to date have concentrated on the characterization of the tensile and fatigue behavior of Al_2O_3 fiber reinforced Mg alloys. In particular, the influences of fiber fraction, fiber orientation, alloy content and loading conditions were investigated.

Major conclusions reached on the program include:

1. Process defects in the form of large clumps of Al_2O_3 grains and fibers that were broken and lying on their sides were preferential sites for crack initiation for both monotonic and cyclic loading along the fiber axis. However, the presence of the defects was not detrimental to axial properties unless the size of the defect was a significant fraction of the specimen cross section. These defects did not play a role in crack initiation during off-axis loading.

2. For CPMg, a relatively weak fiber/matrix interface resulted in a large reduction in off-axis tensile properties. The reduction in strength is related to a change in the mode of fracture from flat fracture across fibers in the axial orientation to failure along the fiber/matrix interface in off-axis orientations. Interfacial failure occurred between the magnesium matrix and the MgO reaction zone.

3. For CPMg, fatigue crack initiation and propagation occurred parallel to the fiber direction but primarily in the magnesium matrix for off-axis loading through the fiber even though the fiber/matrix interface was quite weak. Overload failure in these specimens occurred along the fiber/matrix interface.

4. The critical stress intensity for unstable fracture of off-axis CPMg is controlled by both the normal and shear stress components acting on the fiber/matrix interface.

5. The alloying elements in ZE41A resulted directly in an increased matrix strength and indirectly in an increased fiber/matrix interfacial strength and a decreased fiber strength compared to CPMg.

6. The increased interfacial and matrix strengths combined with the decreased fiber strengths in ZE41A yielded reduced axial and increased off-axis tensile and fatigue properties compared to CPMg. In addition, this change in component strengths delayed the transition from fracture across the fibers to interfacial failure as the angle between the fiber direction and loading axis was increased.

7. The increased interfacial strength was due to a thicker reaction zone of larger MgO particles and not to segregation of alloying elements to the reaction zone. The size of the reaction zone is controlled by the markedly different solidification characteristics of CPMg compared to ZE41A, resulting in considerably different exposure times of the Al_2O_3 fibers to liquid magnesium. This result can possibly be exploited to improve composite mechanical properties through process control.

These results are described in detail in four manuscripts which have either been published or are currently being submitted for publication. These manuscripts are presented as Appendices A-D at the end of this summary. The organization of the Appendices is as follows: Appendix A - "Tensile and Fatigue Behavior of Aluminum Oxide Fiber Reinforced Magnesium Composites: Part I. Fiber Fraction and Orientation" by J. E. Hack, R. A. Page and G. R. Leverant; Appendix B - "Tensile and Fatigue Behavior of Aluminum Oxide Fiber Reinforced Magnesium Composites: Part II. Alloying Effects" by R. A. Page, J. E. Hack, R. Sherman and G. R. Leverant; Appendix C - "Critical Stress Intensity for Off-Axis Fracture of Al_2O_3 Fiber Reinforced Magnesium" by K. S. Chan, J. E. Hack and R. A. Page; and Appendix D - "The Influence of Thermal Exposure on Interfacial Reactions and Strength in Aluminum Oxide Fiber Reinforced Magnesium Alloy Composites" by J. E. Hack, R. A. Page and R. Sherman.

APPENDIX A

"TENSILE AND FATIGUE BEHAVIOR OF ALUMINUM OXIDE FIBER REINFORCED MAGNESIUM COMPOSITES: PART I. FIBER FRACTION AND ORIENTATION"
BY J. E. HACK, R. A. PAGE AND G. R. LEVERANT
PUBLISHED IN METALLURGICAL TRANSACTIONS A,
VOLUME 15A, JULY 1984

TENSILE AND FATIGUE BEHAVIOR OF ALUMINUM OXIDE FIBER REINFORCED MAGNESIUM COMPOSITES: PART I - FIBER FRACTION AND ORIENTATION

J. E. Hack, R. A. Page, and G. R. Leverant

Southwest Research Institute
6220 Culebra Road
San Antonio, Texas 78284, USA

Abstract

The mechanical behavior of commercially pure magnesium reinforced with FP aluminum oxide fibers has been studied as a function of fiber fraction and orientation. Test specimens included material of two different volume fractions of fiber and four different fiber orientations. Axial properties were dependent on the fiber content and generally followed the rule of mixtures. Of the off-axis properties, only the elastic modulus exhibited a significant dependence on fiber content. Off-axis loading resulted in large reductions in both the tensile and fatigue properties. The reductions coincided with a change in fracture morphology from fracture across fibers during axial loading to fracture along the fiber direction for off-axis loading. A weak fiber/matrix interface was found to be responsible for the drop in tensile properties and a combination of a weak matrix and a weak fiber/matrix interface were responsible for the reduced fatigue resistance.

INTRODUCTION

The reinforcement of metal matrices with high strength and high modulus synthetic fibers to produce a hybrid material possessing attractive structural properties is not a new concept. The combination of recently developed high strength and modulus ceramic fibers with lightweight, ductile metal matrices (principally magnesium and aluminum) has spurred renewed interest in the potential of these materials for applications requiring high specific strength and stiffness, toughness and fatigue resistance. Implementation of advanced metal matrix composite materials in structural applications has always suffered, however, due to a lack of a quantitative relationship between microstructure and mechanical behavior.

Although a great deal of work has been performed on fracture mechanisms in metal matrix composites (1-4), the results to date have been quite contradictory in nature. The inconsistencies arise from the complex interaction of the fiber/matrix interfacial region with various applied states of stress. In addition, the presence of the fiber/matrix interface in these composites introduces several mechanisms of crack propagation in addition to those observed in monolithic materials (5). Also, standard metallurgical techniques for modifying the properties of the matrix material (i.e., alloying, heat treatment, deformation processing, etc.) affect the metallurgical structure and properties of the interfacial region as well (6,7). Thus, the effects of processing variables on composite behavior through microstructural changes in the matrix are difficult to separate from the effects of those variables on the fiber/matrix interface.

A research program was initiated to overcome these difficulties by developing quantitative relationships between matrix microstructure, composition,

The specimens utilized for both the tensile and fatigue tests were 15.2 cm long with 1.27 cm x 0.25 cm rectangular cross sections. Machining was performed with the Al_2O_3 fibers lying parallel to the 15.2 cm x 0.25 cm face and oriented at 0, 22.5, 45, and 90° to the 15.2 cm x 1.27 cm face and the tensile axis. Aluminum tabs were bonded to both ends of the specimens for gripping purposes. Strain gages, aligned to measure tensile strains, were attached on opposite faces of the tensile specimens.

The tensile and fatigue tests were both carried out at room temperature in a closed-loop hydraulic testing system. The tensile tests, which yielded information on the effect of fiber volume fraction and fiber orientation on the elastic modulus (E), yield strength (YS), ultimate tensile strength (UTS) and elongation (e) were performed under displacement control at a strain rate of 8.3×10^{-5}/s. Both strain, determined from the strain gages, and load were monitored continuously during testing. Comparison of strain readings from the front and back gages indicated that bending was not significant in these tests. The fatigue tests were run under load control at a frequency of 10 Hz and an R-ratio of 0.1. The number of cycles to failure was determined as a function of maximum stress, fiber volume fraction, and fiber orientation. Tests which did not result in failure in 1 to 2×10^6 cycles were terminated.

RESULTS

Tensile Behavior

The results of the tensile tests, i.e., the YS, UTS, E and e are presented in Table I. It is apparent from these data that fiber orientation affected all four tensile parameters. The most dramatic effect was found in

the YS where a 22.5° misorientation of the fibers decreased the YS by about an order of magnitude. The UTS was also a strong function of fiber orientation, as is evident from Figure 2. In fact, at 90° the YS and UTS had dropped to a value approximately equal to those of sand-cast CP magnesium (21 and 90 MPa, respectively) (8). The elongation showed an abrupt increase as the fiber orientation went from 0° to 22.5° then dropped off with increasing angle for both volume fractions. The ductility in the 55 v/o material tended to be slightly higher at intermediate angles. The elastic modulus was the least sensitive to fiber orientation, exhibiting a factor of two difference between the axial and transverse moduli. The data further indicate that the elastic modulus at all orientations and the axial YS and UTS were increased by increasing the fiber volume fraction. The YS and UTS of off-axis specimens, however, were not sensitive to the fiber volume fraction to any significant degree. The convergence of the UTS curves for 35 and 55 v/o material at 22.5° and beyond in Figure 2 further illustrates the negligible effect that fiber content has on off-axis strength.

Fractographic characterization of the tensile specimens indicated that failure of the axial specimens occurred at 90° to the applied stress, i.e., through the fibers. The role that defects can play in the tensile failure of axial specimens is illustrated by the wide scatter in the axial 55 v/o data. Sample 55-0-A which had a UTS 30% lower than Sample 55-0-B, failed at a massive process defect, roughly 2500 x 200 μm defect. Although Samples 55-0-B, 35-0-A and 35-0-B contained similar defects on the order of ten times the fiber diameter (20 μm), the UTS was in line with previously published values. This implies that defects have to cover a significant fraction of the specimen cross-section to affect tensile properties. The nature of the defects will be discussed in detail in the next section on fatigue behavior.

Failure of all the off-axis 55 v/o samples and the 35 v/o samples tested at 45 and 90° occurred along the fiber axis by decohesion of the fiber/matrix interface. Failure of the 35 v/o samples tested at 22.5° occurred at an angle close to 90° by a mixture of interfacial decohesion and fiber cracking. No evidence of initiation at process defects was found in any of the off-axis tensile specimens.

Fatigue Behavior

The fatigue resistance of both 35 and 55 v/o materials was found to be a function of the fiber orientation. Increasing the angle between the fiber axis and the stress axis resulted in a reduction in the fatigue resistance, as evidenced by the compendium of S-N curves in Figure 3. (The solid and dashed lines in the figure represent a least squares fit to the data. The arrowed data represent samples which had not failed by $\sim 10^6$ cycles and were thus terminated.) As observed in the tensile behavior, the higher volume fraction of fibers resulted in a dramatic increase in the fatigue resistance of the axial specimens. The close grouping of the off-axis data, however, indicates that fiber content did not strongly influence off-axis fatigue strength. The data presented in Figure 3 also indicates that fatigue resistance scales roughly with the UTS. This is more obvious in Figure 4 in which all of the fatigue data, 35 and 55 v/o and axial through transverse geometries, has been normalized with respect to the appropriate UTS. The normalized data all lie within a band which yields an endurance limit, defined as the stress which results in failure in 10^6 cycles, of between 0.6 and 0.95 times the UTS with an average value of about 0.75 times the UTS.

The fatigue and tensile regions of axial fatigue specimens both exhibited fractographic features similar to those of the axial tensile specimens. In both cases cracking occurred across the fibers at roughly 90° to the tensile

axis. The features of the fatigue and overload failures were so similar that it was impossible to determine the extent of fatigue cracking from examinations of the fracture surface. River markings on the fracture surfaces however, indicate that cracking had initiated at process defects. Two distinct types of defects were found to be responsible for fatigue crack initiation: 1) individual fibers which had broken and fallen perpendicular to the stress axis during processing; and 2) large clumps of Al_2O_3 grains which were an order of magnitude larger than the average fiber diameter. Failure of both of these defects was determined (Part II) to be due to delamination of the Al_2O_3/Mg interface. Examples of the two types of defect are shown in Figure 5.

In contrast to the axial specimens, off-axis specimens failed generally parallel to the fiber axis. Furthermore, a striking difference was observed between the fracture morphology of the fatigue and overload regions of the off-axis specimens. This difference is illustrated by the fractographs of Figure 6. The overload regions exhibited features identical to those of the off-axis tensile failures, as would be expected. Delamination of the fiber/ matrix interface was the primary mode of failure in all but the 35 v/o material oriented at 22.5°. Thus, the fracture was oriented along the fiber axis in all but the 35 v/o material oriented at 22.5°. The overload failure mode was mixed in these samples, consisting of roughly equal amounts of interfacial delamination and flat fracture across fibers, and occurred approximately perpendicular to the tensile axis.

Fatigue cracking in all of the off-axis specimens occurred along the direction of the fiber axis by a combination of delamination of the fiber/matrix interface and cracking of the magnesium matrix. Of these, matrix cracking, which exhibited a brittle, crystallographic morphology reminiscent of cyclic

cleavage (9), as in Figure 7, was the predominant mode. In many instances the crystallographic features were maintained over distances corresponding to from tens to hundreds of fiber diameters. Figure 8 is typical of one such area. Examination of the fatigue regions did not indicate that process defects acted as initiation sites as they had in the axial tests. Metallographic sections taken through a number of the fatigue regions revealed numerous secondary cracks, many of which were entirely situated in matrix material. An example of the secondary cracking observed is presented in Figure 9.

Fiber Spacing

Average fiber spacings were determined from fatigue and overload regions of both 35 and 55 v/o material by counting the number of fibers intersected by lines of known length passed randomly in the fracture plane and perpendicular to the fiber axis. For comparison purposes, average spacings were also determined on metallographic sections cut transverse to the fiber axis. In this case the lines were passed randomly in a plane perpendicular to the fiber axis. The data, which represent averages obtained from 3 to 10 separate counts, are presented in Table II. Spacing obtained from fatigue regions were consistently larger than those obtained from random transverse sections. On the other hand, spacings obtained from the overload regions were consistently smaller than those obtained from random transverse sections.

Auger Spectroscopy

A number of transverse specimens were fractured in situ in a Physical Electronics 595 scanning Auger microprobe. The in-situ fracture occurred along fiber/matrix interfaces, Figure 10, in a manner similar to the off-axis tensile and overload failures. Spectra taken from the fiber trough and the fiber surface are presented in Figures 11a and b, respectively. Comparsion of the fine structure of the magnesium peaks and the ratio of the oxygen to magnesium peak

heights with spectra taken from laboratory standards (10) indicate that the trough side of the fracture was metallic magnesium with a small amount of oxygen and the fiber side of the fracture was an oxide of magnesium, most likely MgO. Aluminum was not detected on either the trough or the fiber surface.

DISCUSSION

As mentioned in the introduction, Al_2O_3 fiber reinforced magnesium was chosen for this investigation because it was representative of the most recent generation of composite materials which contain high performance, state-of-the-art fibers in a ductile metal matrix. The test results obtained for the Al_2O_3 fiber reinforced commercially pure magnesium indicate the effect of fiber orientation and volume fraction on tensile and fatigue properties and provide a basis from which the effects of changes in various material parameters such as matrix alloying and fiber/matrix interfacial strength can be evaluated.

Tensile Behavior

The tensile results indicate that Al_2O_3 fiber reinforced magnesium tested in the axial direction responds to changes in fiber content in much the same manner as other composites which have been investigated (11-13), i.e., YS, UTS, and E increase with increased fiber content. This behavior is consistent with the trend predicted by the rule of mixtures (ROM). Although the ROM values for UTS were quite close to those observed for axial specimens, E was overestimated by approximately ten percent for both 35 and 55 v/o materials. The ROM calculations were made with UTS Mg = 90 MPa (14); UTS Al_2O_3 = 965 MPa (15); E Mg = 45 GPa (14); E Al_2O_3 = 384 GPa (15).

The off-axis results illustrate the dramatic effect that fiber orientation can have in composites of this type. Large drops in YS, UTS, and E were

pure matrix material. Although failure in tensile overload occurred along the weak fiber/matrix interface in off-axis specimens, subcritical fatigue

observed at all misorientations tested. In the transverse direction the UTS had dropped to a value equal to or slightly below that of the matrix alone. The modulus, however, was approximately doubled by the presence of the fibers. The sharp reduction in UTS and YS was related to a change in failure mode from flat fracture across fibers to delamination of the fiber/matrix interface.

Resolution of the stresses into the fiber axis, interface normal and interface shear components yields (16):

$$\sigma_{11} = \sigma_A \cos^2\theta \qquad [1]$$

$$\sigma_{22} = \sigma_A \sin^2\theta \qquad [2]$$

$$\sigma_{12} = \frac{\sigma_A}{2} \sin^2\theta \qquad [3]$$

respectively, where σ_A is the applied stress. A plot of normalized stress versus angle is given in Figure 12.

If the interfacial strength was a significant fraction of the fiber strength, the composite tensile strength would be expected to increase with misorientation angle. Interfacial shear controlled failure would cause the UTS to fall with increasing θ up to 45° and then rise as θ increased to 90°. If the off-axis failure occurred due to normal stresses, however, the UTS would be expected to show a constant decrease with increasing θ. The lack of shearing in the troughs of failed off-axis specimens and the tensile behavior shown in Figure 2 strongly support the ideas that the interface is very weak with respect to normal forces. Even at 22.5° where σ_{11}/σ_A and σ_{22}/σ_A are 0.85 and 0.15, respectively, the weakness of the interface in comparison with the axial

composite strength is dramatic enough to induce predominantly interfacial failure. An independent analysis based on stress intensity factors also clearly shows the dominant role of the normal stress (17).

A similar analysis for strains can be used to explain the elongation behavior. Since macroscopic deformation is restricted to occur parallel to the fiber orientation in off-axis specimens, the shear strain would be expected to control the ductility of the composite. As can be seen from Figure 13 (16), the interfacial shear strains in a unidirectional composite increase abruptly with Θ as the angle of misorientation increases from 0° and then falls off slowly with increasing Θ. This is precisely the behavior in e observed in Table I.

The Auger results indicate that off-axis failure occurs along a magnesium/magnesium oxide interface, which must be concluded to be the matrix/reaction zone interface. Formation of magnesium oxide in the reaction zone is predicted by thermodynamic considerations, as is the formation of $MgAl_2O_4$ spinel. Levi et al. (18) have shown that MgO can form when the magnesium content of the matrix is high. Thus, it can be concluded that a reaction zone of MgO formed during casting and that the interface between the reaction zone and the matrix was the site of off-axis failure. The nature of the interface region is discussed in Part II of this pair of papers.

The insensitivity of the off-axis YS and UTS to changes in fiber content is also noteworthy. Similar behavior has been observed when matrix failure predominates (13). On the other hand, a strong dependence on fiber content has been observed when failure occurs by fiber splitting (11). These observations suggest that, unless the fibers participate in off-axis failure, the off-axis YS and UTS do not benefit greatly from increases in the fiber volume fraction. Large benefits would be expected, however, from increases in the fiber/matrix

interface strength. This has been observed with an alloyed Mg matrix reinforced with Al_2O_3 and is reported in Part II.

Fatigue Behavior

The fatigue resistance of the Al_2O_3 fiber reinforced magnesium, as measured by S-N curves, mirrored the UTS. Hence, all of the correlations that were made between fiber content or orientation and tensile strength also apply to the fatigue life behavior. Increases in fiber content would therefore be expected to increase lifetimes in axial fatigue but provide little or no benefit for off-axis loadings, as was observed. Similarly, increases in misorientation angle were found to sharply depress the S-N curves.

One of the most interesting aspects of this study was the off-axis subcritical fatigue crack growth behavior. Although the fiber/matrix interface was weak, as demonstrated by the off-axis tensile and overload failures, fatigue cracking occurred primarily through the magnesium matrix.* The matrix cracking, which was brittle and crystallographic in appearance, may be similar to the crystallographic Stage I cracking which has been observed along slip planes and twin boundaries in monolithic magnesium (19). The major role of the fibers in fatigue is believed to be one of channeling the fatigue cracks in a direction parallel to the fiber axis, although interfacial delamination did play at least a minor role in the cracking.

---

* The observation that fatigue cracking occurred primarily through the matrix is supported by the fractography, Figures 9 and 11, the larger than average fiber spacing observed on the fracture surfaces, Table II, and the observations of the secondary cracks situated entirely in the matrix, Figure 12. Furthermore, sections through the thumbnails indicated that the fatigue cracks tended to step around fibers.

All the off-axis tensile data indicates that the interface between the fiber and matrix is extremely weak. Since fatigue cracks appear to have initiated in the matrix and only showed a transition to interfacial failure at overload, it is safe to assume that initiation occurred early in the lifetime. Thus, the lifetime of the off-axis specimens was propagation controlled even in the high cycle regime. From the geometry of the thumbnails, it is known that the stress intensity did not exceed approximately 35 MPa$\cdot\sqrt{m}$ during the off-axis fatigue tests (17). Crack growth rates in monolithic Mg alloys have been found to be on the order of 10^{-8} m/cycles at these levels of stress intensity (20). Similar behavior has been found in nickel base superalloy single crystals (21) and other metal-matrix composite systems (22) where initiation occurs early in life but fatigue crack growth rates at the critical stress intensity are still close to the near-threshold regime.

The implications of these results are twofold. First, fiber/matrix interface strength should play a primary role in the off-axis S-N behavior through its control of overload resistance but only a secondary role in the off-axis fatigue crack propagation behavior since the primary fracture morphology was not interface related. Second, matrix strength should play a primary role in both off-axis S-N behavior and fatigue crack propagation since it controls the primary fracture morphology. Alloying of the matrix therefore appears to be the most promising approach to improved off-axis properties since, through proper alloy additions, it may be possible to increase both matrix and interfacial strengths.

Process Defects

The fractographic results on the axial tensile and fatigue specimens indicated that process defects play a role in crack initiation at 0°. In fact, fatigue crack initiation could always be traced to a process defect. However,

the UTS of the composite only deviated from the role of mixtures when an unusually large defect was present (Figure 3). Defects of this size were not found in any other specimen. Although fatigue crack initiation most likely occurred early in the specimen lifetime due to the presence of the process defects, the endurance limit in the axial fatigue specimens remained at approximately 70% of the ROM UTS value. This was the same range as was found for the off-axis specimens where process defects did not contribute to crack initiation. In addition, most component design considerations incorporate cross-plied fibers to offset the inferior off-axis tensile strength with respect to the axial orientation, thus providing paths for crystallographic crack initiation in the matrix. With all of these facts taken into account, it seems that, with the exception of gross defects such as that found in the 55 v/o axial tensile specimen, the improvement in mechanical properties to be gained by the removal of the process defects would not be worth the considerable cost and effort required. Some form of non-destructive evaluation to detect gross defects is required, however.

CONCLUSIONS

The following conclusions can be drawn from the results obtained in the present investigation.

(1) Process defects in the form of large clumps of Al_2O_3 grains and fibers which were broken and lying on their sides were preferential sites for crack initiation for both monotonic and cyclic loading along the fiber axis. However, the presence of the defects was not particularly damaging to axial tensile or fatigue properties unless

the size of the defect was a significant fraction of the specimen cross-section. Process defects did not play a role in crack initiation during off-axis loading.

(2) Changes in the fiber content can be used to alter the axial properties. With respect to the off-axis properties, however, only the modulus is significantly affected by fiber content.

(3) The weak fiber/matrix interface causes a large reduction in tensile properties when loading is off-axis. The reduction in properties is related to a change in the mode of fracture from flat fracture across fibers in the axial condition to failure along the fiber/matrix interface in the off-axis condition. An increase in interfacial strength brought about either through process modification or through alloying should yield improved off-axis properties.

(4) Interfacial delamination, which was the predominant failure mode in all off-axis overload failures, occurred along the interface between the magnesium matrix and the magnesium oxide reaction zone.

(5) Fatigue crack initiation and propagation during off-axis loading occurs primarily through the magnesium matrix. Hence, alloy additions designed to increase the strengths of the matrix and the fiber/matrix interface should be effective in increasing the off-axis fatigue resistance of the composite.

ACKNOWLEDGEMENTS

The authors are grateful for the support of this work by the Army Research Office under Contract No. DAAG29-81-K-0049. We would also like to thank Dr. R. Sherman for performing the Auger analyses. The technical assistance of Messrs. V. D. Aaron and H. Saldana in specimen preparation and testing is also greatly appreciated.

REFERENCES

1. G. A. Cooper and A. Kelly: J. Mech. Phys. of Solids, 1967, Vol. 15, p. 279.
2. R. E. Cooper: J. Mech. Phys. Solids, 1970, Vol. 18, p. 179.
3. A. Kelly: Proc. Royal Soc. London, 1970, Vol. 319, p. 95.
4. D. L. McDanels, R. W. Jech, and J. M. Weeton: Trans. TMS-AIME, 1965, Vol. 233, p. 636.
5. A. S. Tetelman: Composite Materials: Testing and Design, ASTM STP 460, p. 473, American Society for Testing and Materials, Philadelphia, PA, 1969.
6. J. R. Hancock: Composite Materials: Testing and Design (Second Conference), ASTM STP 497, p. 483, American Society for Testing and Materials, Philadelphia, PA, 1972.
7. G. D. Swanson and J. R. Hancock: Composite Materials: Testing and Design, (Second Conference), ASTM STP 497, p. 469, American Society for Testing and Materials, Philadelphia, PA, 1972.
8. Metals Handbook, 9th ed., Vol. 2, p. 264, American Society for Metals, Metals Park, OH, 1979.
9. M. Gell and G. R. Leverant: Acta Met., 1968, Vol. 16, p. 553.
10. L. E. Davis, N. C. MacDonald, P. W. Palmberg, G. E. Riach, and R. E. Weber: Handbook of Auger Electron Spectroscopy, 2nd ed., pp. 39-41, Physical Electronic Industries, Eden Prairie, MN, 1976.
11. K. M. Prewo and K. G. Kreider: Met. Trans, 1972, Vol. 3, p. 2201.
12. P. E. Chen and J. M. Lin: Mat. Res. Std., 1969, Vol. 9, No. 8, p. 29.
13. K. M Prewo and K. G. Kreider: J. Comp. Mat., 1972, Vol. 6, p. 338.

14. Metals Handbook, 8th ed., Vol. 1, American Society for Metals, Metals Park, OH, 1961.

15. R. T. Pepper and D. C. Nelson: Report No. NASA CR-167999, NASA-Lewis Research Center, Cleveland, OH, September 1982.

16. C. C. Chamis and J. H. Sinclair: Report No. NASA TN D-8215, NASA-Lewis Research Center, Cleveland, OH, April 1976.

17. K. S. Chan, J. E. Hack, and R. A. Page: "Critical Stress Intensity for Off-Axis Fracture of Al_2O_3 Fiber Reinforced Magnesium," (in press) Metallurgical Transactions.

18. C. G. Levi, G. J. Abbaschian, and R. Mehrabian: Met. Trans., 1978, Vol. 9A, p. 697.

19. M. J. May and R. V. K. Honeycombe: J. Inst. Metals, 1963-64, Vol. 92, p. 41.

20. N. M. Grinberg, Inst. J. Fatigue, 1982, Vol. 4, p. 83.

21. M. Gell and G. R. Leverant, Trans. TMS-AIME, 1968, Vol. 242, p. 1869.

22. M. Gouda, K. M. Prewo and A. J. McEvily: Fatigue of Fibrous Composite Materials, ASTM STP 723, K. N. Lauritis, ed., pp. 101-115, American Society for Testing Materials, Philadelphia, PA, 1981.

TABLE I

TENSILE PROPERTIES OF 35 AND 55 V/O AL_2O_3
FIBER REINFORCED CP MAGNESIUM

v/o Al_2O_3	Orientation, deg.	YS, MPa	UTS, MPa	E, GPa	e_f, %
35	0 (axial)	213	383 (396)	149 (162)	.26
35	22.5	34	207	116	.52
35	45	23	108	90	.45
35	90 (transverse)	21	104	85	.42
55	0 (axial)	321*	567* (571)	197 (229)	.30*
55	22.5	27	196	155	.81
55	45	30	157	124	.58
55	90 (transverse)	18	67	90	.24

All values are the averages of duplicate tests except where noted.
Values in parenthesis are calculated from the rule-of-mixtures (ROM).
* Values from a single test. Second specimen failed at 400 MPa due to the presence of a large process defect.

TABLE II

FIBER SPACING COMPARISON IN
FATIGUE AND OVERLOAD FAILURE

v/o Fiber	Orientation	Location	Average Spacing, μm
35	-	Transverse Section	44
35	-	Transverse Section	37
35	45°	Fatigue Region	74
35	45°	Fatigue Region	197
35	45°	Overload Region	23
35	90°	Fatigue Region	74
35	90°	Fatigue Region	60
35	90°	Fatigue Region	75
35	90°	Overload Region	24
55	-	Transverse Section	29
55	-	Transverse Section	30
55	22.5°	Fatigue Region	43
55	22.5°	Overload Region	24
55	45°	Fatigue Region	46
55	45°	Overload Region	20
55	90°	Fatigue Region	35
55	90°	Overload Region	21

LIST OF FIGURE CAPTIONS

Figure 1. Polished and etched transverse section of 35 v/o Al_2O_3 fiber reinforced CP Mg. Note large grains present as in Area A.

Figure 2. Effect of fiber orientation on ultimate tensile strength for both 35 and 55 v/o Al_2O_3 fiber reinforced CP Mg.

Figure 3. Combined S-N curves for both 35 and 55 v/o Al_2O_3 fiber reinforced CP Mg illustrating the effect of fiber volume fraction as a function of orientation.

Figure 4. Fatigue data for both 35 and 55 v/o Al_2O_3 fiber reinforced CP Mg normalized with respect to the UTS.

Figure 5. Typical process defects responsible for crack initiation in axial specimens: Al_2O_3 fiber reinforced CP Mg (a) transverse fibers (Area 1), and (b) clumps of Al_2O_3 grains (Area 2).

Figure 6. Scanning electron micrographs of typical overload (a) and fatigue (b) failures in off-axis specimens of Al_2O_3 fiber reinforced CP Mg. Note that the failure in overload occurs almost exclusively along fiber/matrix interfaces while subcritical fatigue crack growth occurs parallel to the interfaces but primarily through the matrix.

Figure 7. High magnification view of typical cleavage-like matrix fracture morphology in fatigue thumbnail regions of off-axis specimens of Al_2O_3 fiber reinforced CP Mg. Fiber trough is visible in region 1.

Figure 8. Scanning electron micrograph of typical off-axis fatigue region illustrating the large distances over which crystallographic features extend.

Figure 9. Scanning electron micrograph of a typical secondary crack located in the matrix of an off-axis fatigue specimen of Al_2O_3 fiber reinforced CP Mg. Note that the cracking avoids fiber/matrix interfaces during subcritical crack growth (crack path denoted by arrows).

Figure 10. Scanning electron micrograph of the failure obtained in the scanning auger microprobe. Typical exposed fiber in Area A, fiber trough in Area B.

Figure 11. Auger electron spectra taken from the fiber trough (a) and the fiber surface (b) of an in-situ fractured specimen.

Figure 12. Variation of material axes stress in unidirectional composite plotted against load direction [Ref. 16].

Figure 13. Variation of material axes strains in a typical unidirectional composite plotted against load direction [Ref. 16].

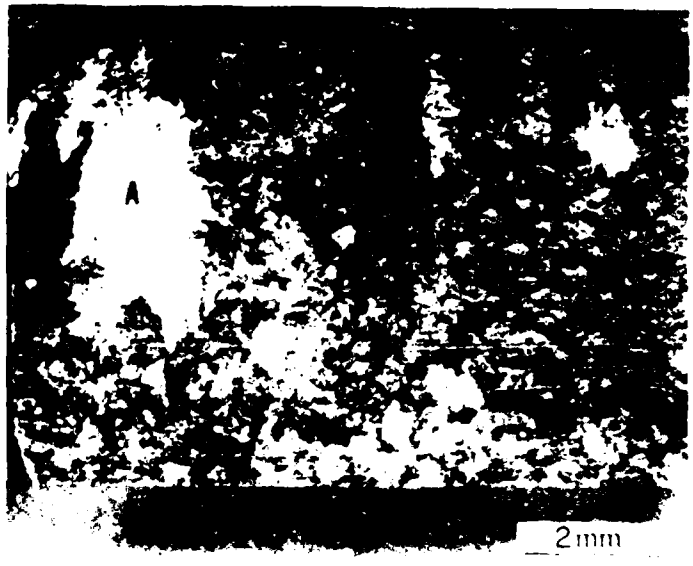

Figure 1. Polished and etched transverse section of 35 v/o Al_2O_3 fiber reinforced CP Mg. Note large grains present as in Area A.

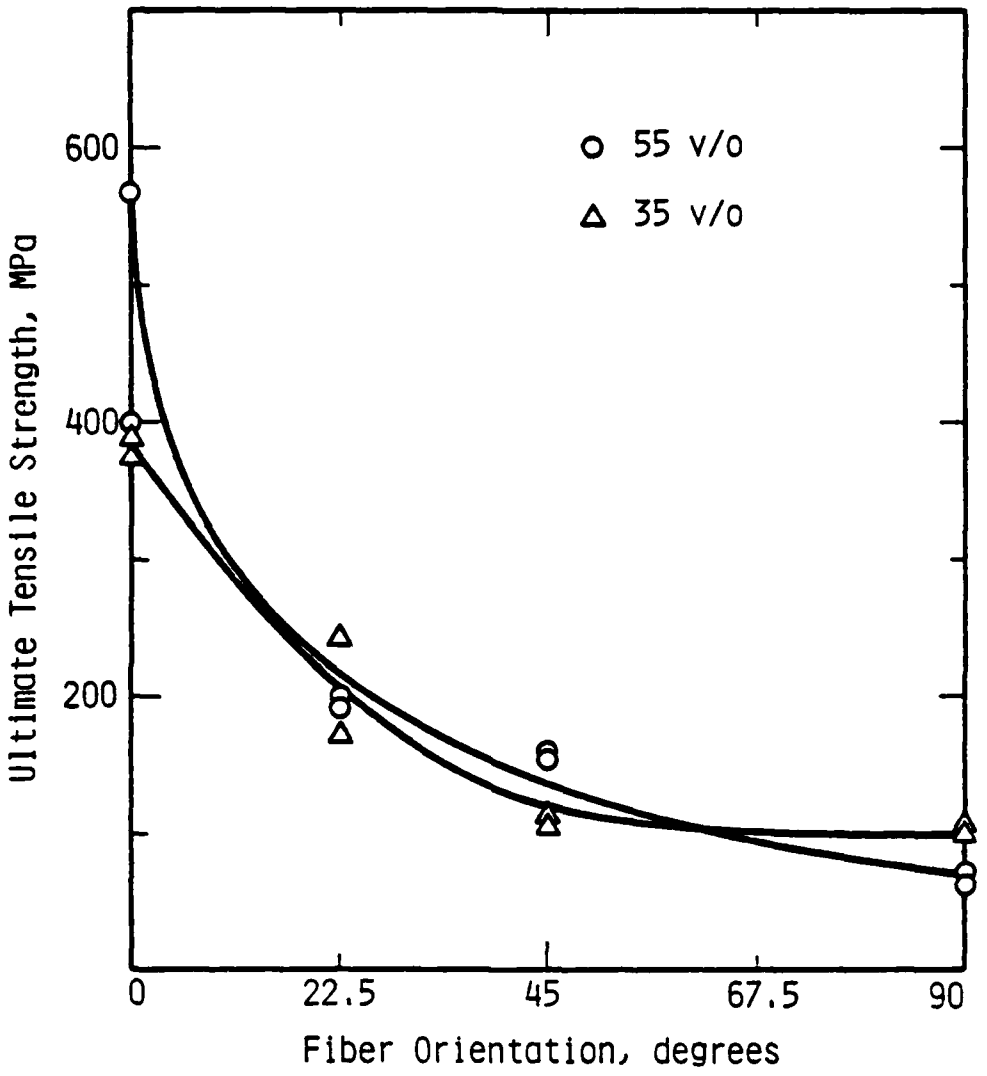

Figure 2. Effect of fiber orientation on ultimate tensile strength for both 35 and 55 v/o Al_2O_3 fiber reinforced CP Mg.

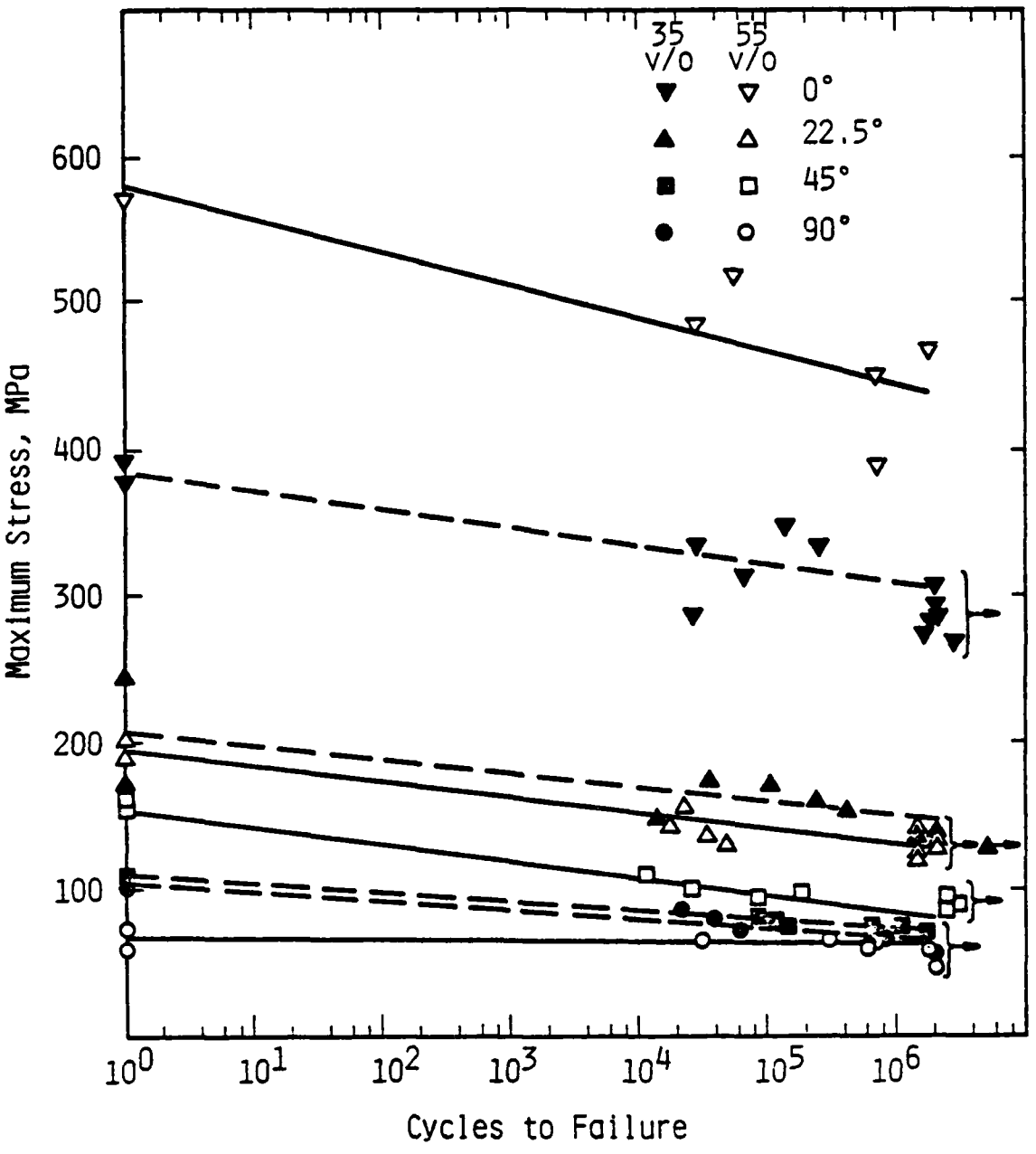

Figure 3. Combined S-N curves for both 35 and 55 v/o Al_2O_3 fiber reinforced CP Mg illustrating the effect of fiber volume fraction as a function of orientation.

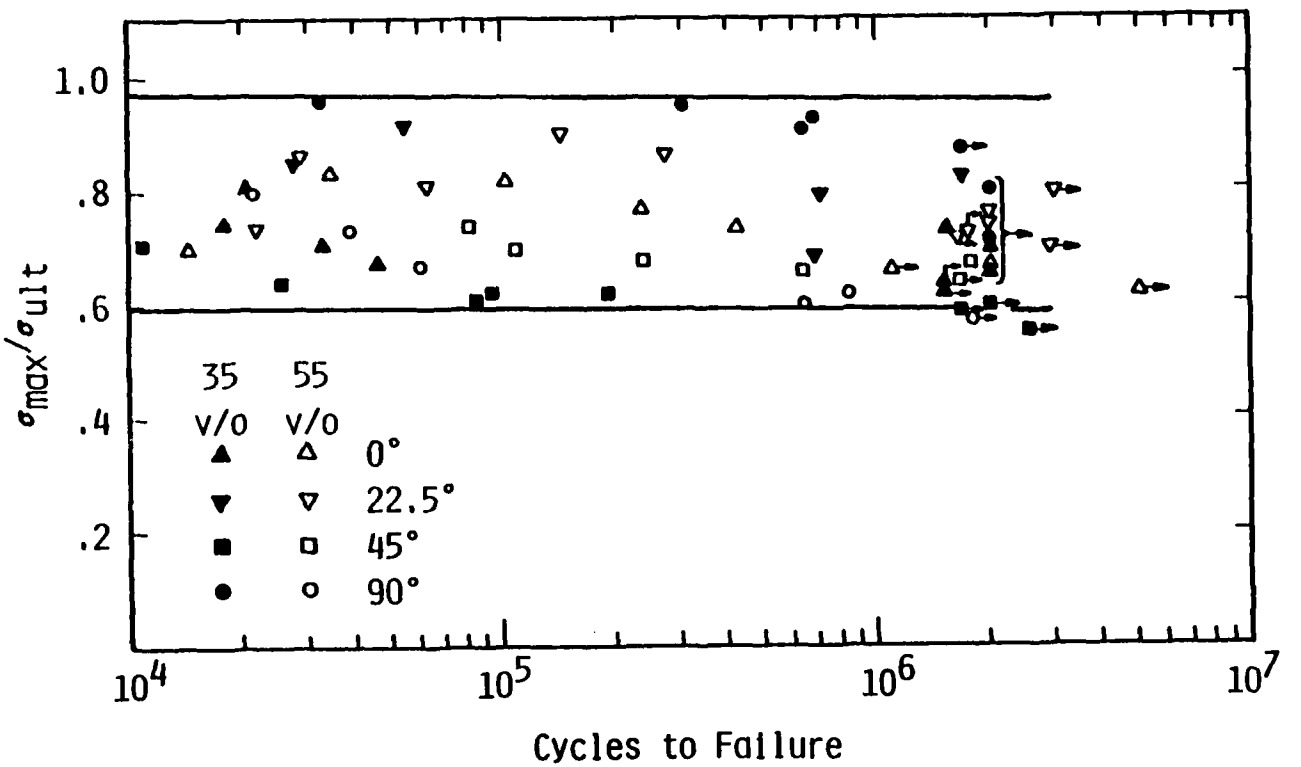

Figure 4. Fatigue data for both 35 and 55 v/o Al_2O_3 fiber reinforced CP Mg normalized with respect to the UTS.

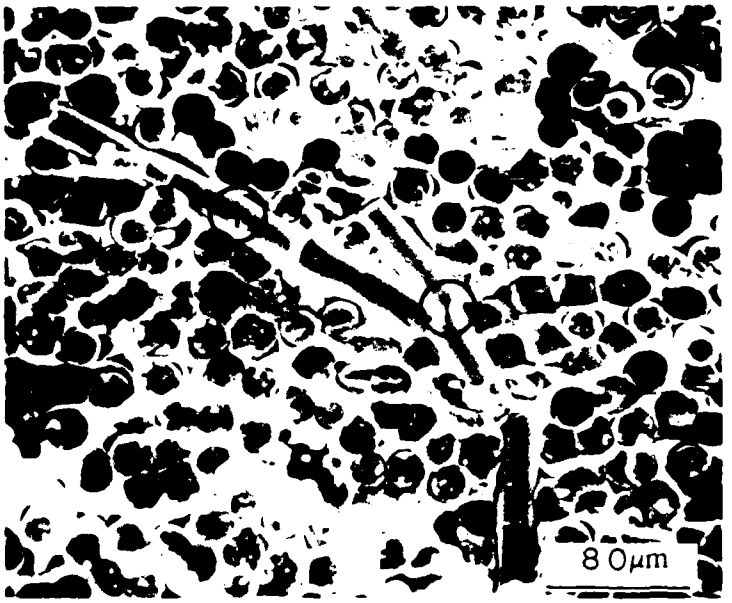

(a)

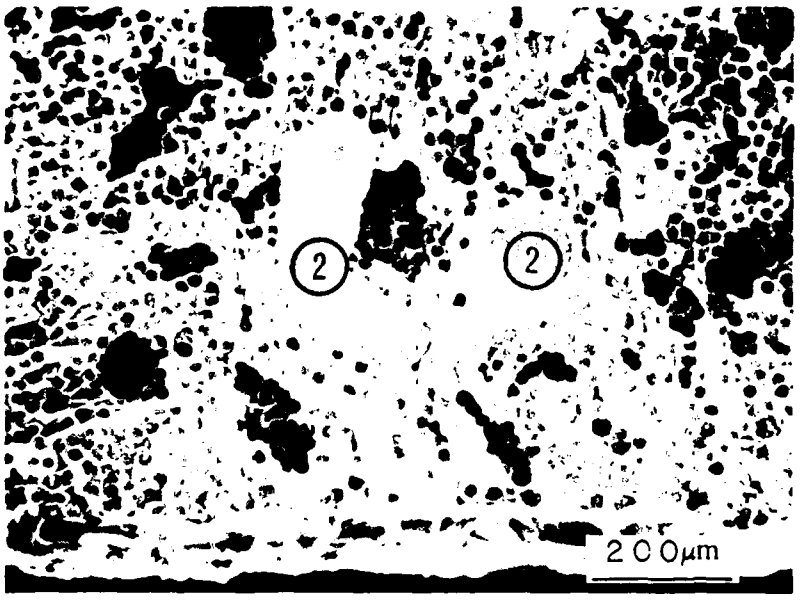

(b)

Figure 5. Typical process defects responsible for crack initiation in axial specimens: Al_2O_3 fiber reinforced CP Mg (a) transverse fibers (Area 1), and (b) clumps of Al_2O_3 grains (Area 2).

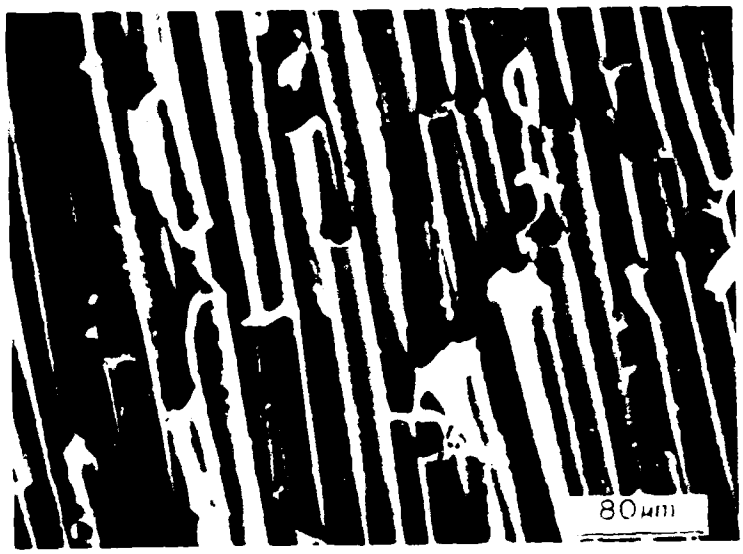

(a)

(b)

Figure 6. Scanning electron micrographs of typical overload (a) and fatigue (b) failures in off-axis specimens of Al_2O_3 fiber reinforced CP Mg. Note that the failure in overload occurs almost exclusively along fiber/matrix interfaces while subcritical fatigue crack growth occurs parallel to the interfaces but primarily through the matrix.

Figure 7. High magnification view of typical cleavage-like fracture morphology in fatigue thumbnail regions of off-axis specimens of Al_2O_3 fiber reinforced CP Mg. Fiber trough is visible in region 1.

Figure 8. Scanning electron micrograph of typical off-axis fatigue region illustrating the large distances over which crystallographic features extend.

Figure 9. Scanning electron micrograph of a typical secondary crack located in the matrix of an off-axis fatigue specimen of Al_2O_3 fiber reinforced CP Mg. Note that the cracking avoids fiber/matrix interfaces during subcritical crack growth (crack path denoted by arrows).

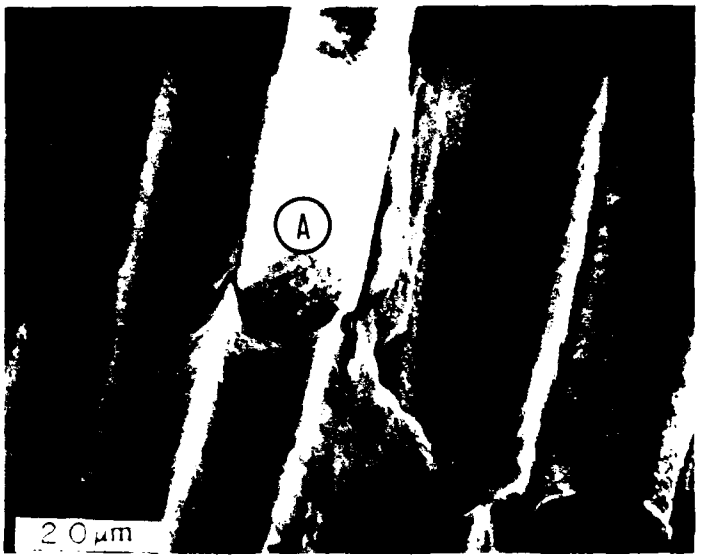

Figure 10. Scanning electron micrograph of the failure obtained in the scanning auger microprobe. Typical exposed fiber in Area A, fiber trough in Area B.

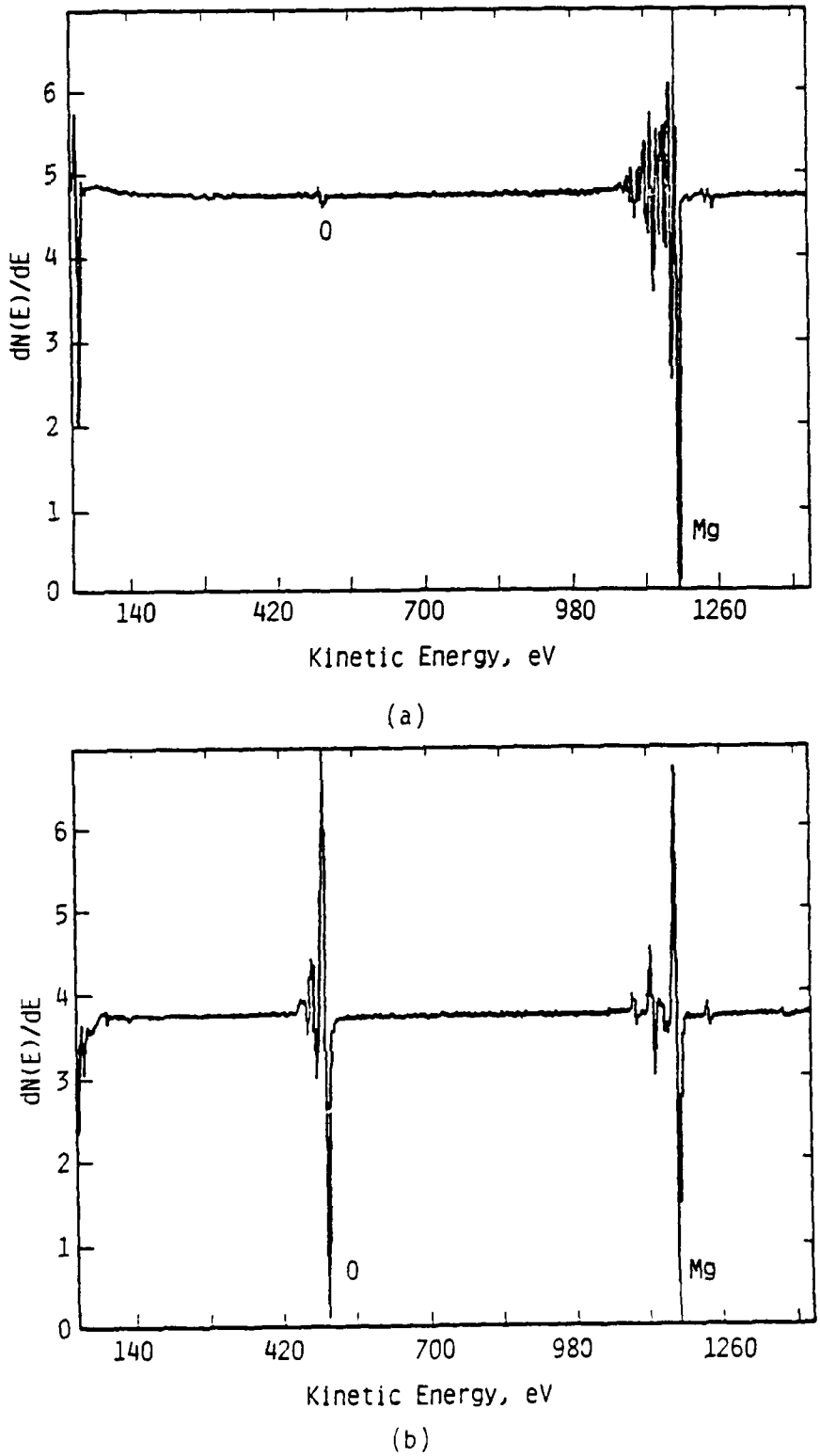

Figure 11. Auger electron spectra taken from the fiber trough (a) and the fiber surface (b) of an in-situ fractured specimen.

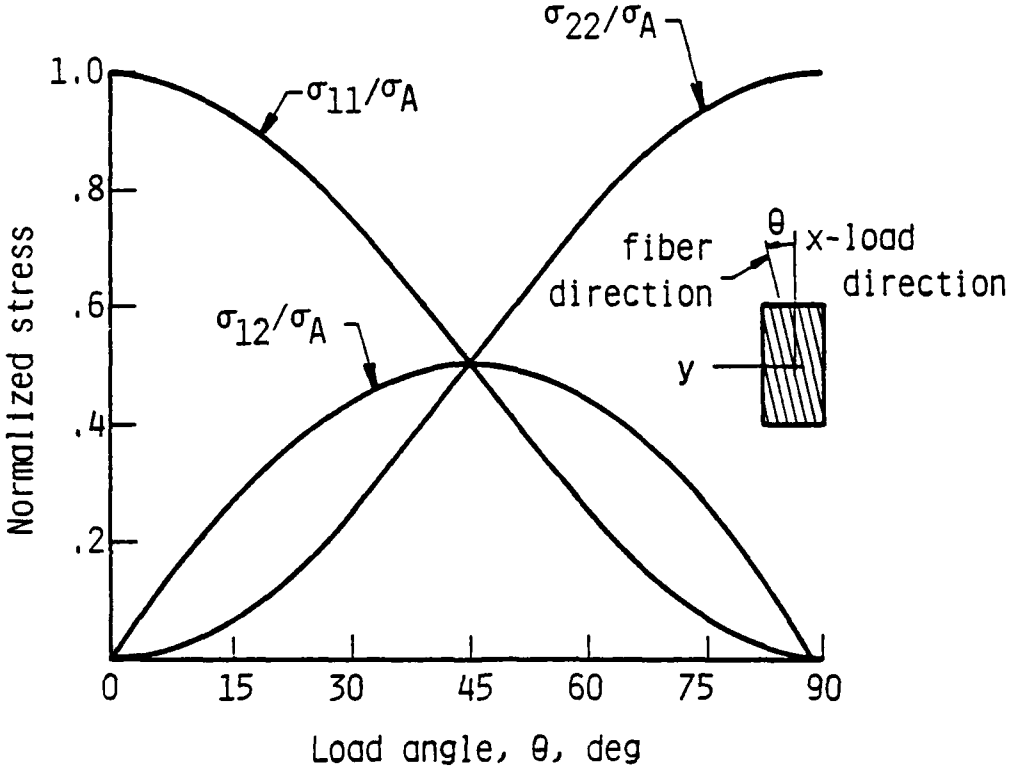

Figure 12. Variation of material axes stress in unidirectional composite plotted against load direction [Ref. 16].

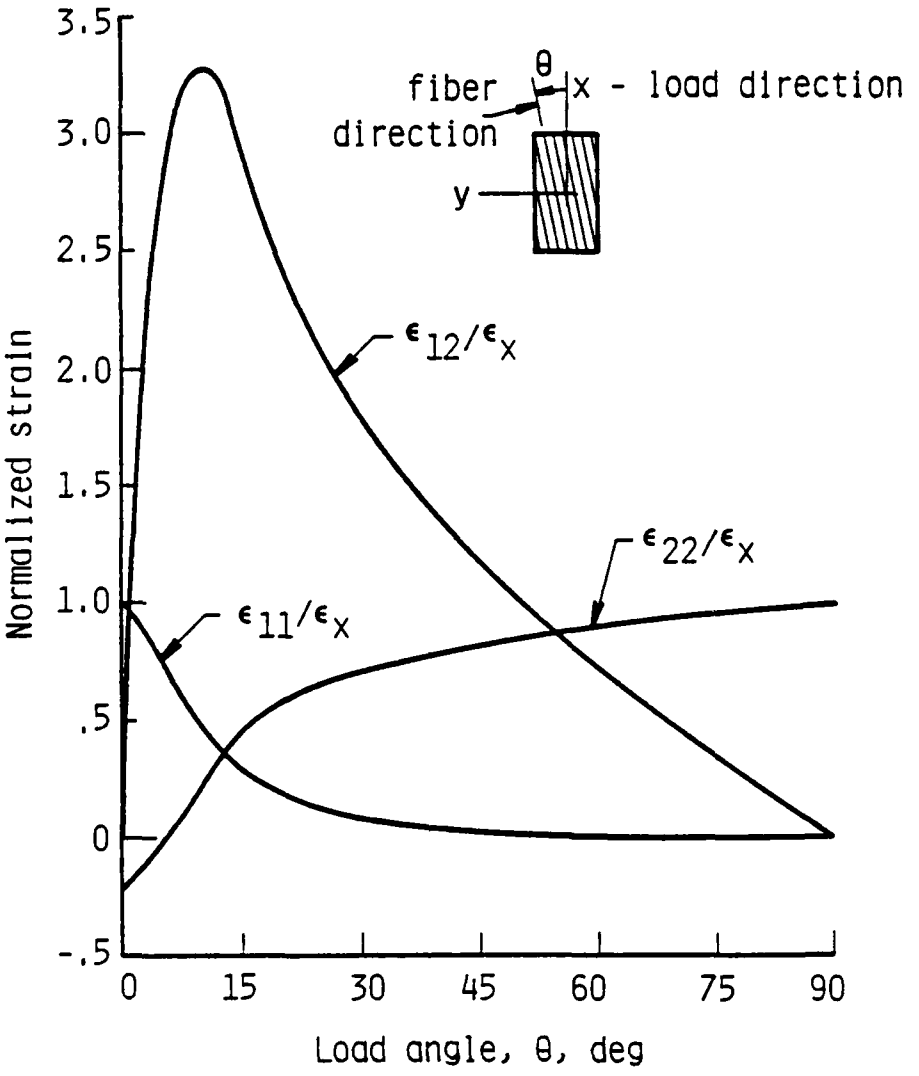

Figure 13. Variation of material axes strains in a typical unidirectional composite plotted against load direction [Ref. 16].

APPENDIX B

"*TENSILE AND FATIGUE BEHAVIOR OF ALUMINUM OXIDE FIBER REINFORCED* MAGNESIUM COMPOSITES: PART II. ALLOYING EFFECTS"
BY R. A. PAGE, J. E. HACK, R. SHERMAN AND G. R. LEVERANT
PUBLISHED IN METALLURGICAL TRANSACTIONS A,
VOLUME 15A, JULY 1984

TENSILE AND FATIGUE BEHAVIOR OF ALUMINUM OXIDE FIBER REINFORCED MAGNESIUM COMPOSITES: PART II - ALLOYING EFFECTS

R. A. Page, J. E. Hack, R. Sherman and G. R. Leverant

Southwest Research Institute
6220 Culebra Road
San Antonio, Texas 78284, USA

Abstract

The effect of matrix alloy additions on mechanical properties was examined by comparing the tensile and fatigue properties of commercially pure magnesium and ZE41A (Mg-4.25 Zn-0.5 Zr-1.25 RE) which were both reinforced with FP aluminum oxide fibers. The alloy additions were found to improve the off-axis properties but decrease the axial properties. This was brought about by an increase in the matrix and interfacial strengths and a decrease in the fiber strength. It was also determined that the reaction zone in both materials was MgO and that strengthening of the interface was due to an increased particle size and/or a thicker reaction zone and not to any segregation of alloying elements to the interface.

INTRODUCTION

The important effect that matrix composition and heat treatment have on off-axis properties has been demonstrated in a number of metal matrix composite systems (1,2). Generally, these variables have not been found to influence axial properties. Although some attempts have been made to correlate matrix composition and heat treatment with corresponding changes in the toughness of the composite (1), no quantitative correlations have been made with the local decohesion stress. In addition, effects of microstructural changes in the matrix have not been successfully separated from residual stress and interfacial effects.

A recent study (presented in in Part I) of the fatigue and tensile behavior of a model material (FP Al_2O_3 fibers in a commercially pure Mg Matrix) indicated that off-axis fatigue and tensile properties were suppressed because of the combination of a low fiber/matrix interfacial strength and a soft matrix. Under either cyclic or static loading the drastic drop in fatigue and tensile properties with angle was found to correspond with a change in failure mode from flat fracture across the fibers under axial loading conditions to interfacial and/or matrix failure along the fiber orientation for off-axis loading. One of the conclusions of the study was that alloy additions designed to increase the strength of the fiber/matrix interface and/or the strength of the matrix should improve off-axis properties. It has also been found that the transverse strength is dependent on matrix composition in FP/Mg composites (3). It was not known whether this phenomenon was purely a matrix strengthening effect or due to a subtle change in interfacial structure.

This paper reports the initial results of a study of the influence of matrix composition on the micromechanisms of fracture and the tensile and

fatigue properties of Al_2O_3 fiber reinforced magnesium composites. This work and earlier work on the model material (Part I) provide the foundation for a continuing program designed to develop quantitative relationships between matrix microstructure, composition, and properties; fiber orientation and volume percent; and fatigue crack growth behavior in these materials through direct observations of the effects of these variables on the strain field at the tip of a growing crack.

EXPERIMENTAL

The effect of matrix alloy content was investigated by comparing the fatigue and tensile properties of two materials which differed only in the composition of the matrix. Commercially pure magnesium (CPMg) was utilized as the baseline matrix material while ZE41A, a magnesium alloy with approximately 4.25 wt.% Zn, 0.5 wt.% Zr, and 1.25 wt.% rare earths, was chosen to represent alloyed matrix materials. Both materials contained 55 v/o of continuous, unidirectional, 20 μm diameter Al_2O_3 fibers. The composite plates were manufactured by E. I. DuPont de Nemours and Co. by liquid infiltration of the FP Al_2O_3 fibers.

Specimens 15.2 cm long with 1.27 cm x 0.25 cm rectangular cross sections were used for both the tensile and fatigue tests. The specimens were machined with the Al_2O_3 fibers lying parallel to the 15.2 cm x 0.25 cm face and oriented at angles of 0, 22.5, 45 and 90° and 0 and 22.5° to the tensile axis for CPMg and ZE41A, respectively. Gripping was facilitated by the addition of aluminum tabs which were epoxied to both sides of the specimen ends.

A closed-loop hydraulic testing system was used for all of the mechanical tests. The fatigue tests were run under load control at an R-ratio of 0.1

and a frequency of 10 Hz. Samples were tested to failure or to approximately 10^6 cycles, whichever came first. The tensile tests were performed under displacement control at a strain rate of 8.3×10^{-5}/s. Specimen strain was determined from strain gages which were attached to opposite faces of the tensile specimens.

Auger Spectroscopy

To gain a better understanding of the effect of matrix composition on the fiber/matrix interface, transverse specimens of both CPMg and ZE41A were fractured in situ and examined in a Physical Electronics 595 scanning Auger microprobe. Surface spectra were taken with an incident accelerating voltage of 5 KeV and beam currents ranging from 0.3 μA to greater than 1 μA. Spectra were obtained in point mode, with a beam size of approximately 1 μm, and with the TV raster operating. All operating methods produced the same results within the chosen signal-to-noise conditions. A limited amount of ion sputtering was also performed.

Transmission Electron Microscopy

Thin foils of both composite materials were prepared by ion milling and examined in a Philips 301 scanning transmission electron microscope. Microdiffraction patterns were obtained by limiting the specimen area illuminated with a focused second condenser aperture (4). A 5 μm aperture was used which, with the demagnification of 38 times obtained in the Philips 301 STEM, yielded an illuminated area of approximately 130 nm in diameter. Diffraction patterns were taken at multiple orientations so that the interface particles could be unambiguously identified.

RESULTS

Tensile Behavior

It is clear from the tensile data, Table I and Figure 1, that the alloy additions to the matrix had a strong influence on both the yield, YS, and ultimate tensile, UTS, strengths. Under axial loading, the use of ZE41A as a matrix material rather than CPMg resulted in approximately a 50 percent increase in YS and a 15 percent decrease in UTS. At 22.5° the ZE41A material demonstrated increased YS and UTS with the UTS increased by about a factor of two and the YS by an order of magnitude over the CPMg material. As expected, the elastic modulus at 0 and 22.5° was not significantly affected by the alloy additions. Thus the alloy additions in ZE41A, i.e., Zn, Zr, and rare earths, benefitted the off-axis tensile properties and the axial yield strength but reduced the axial UTS.

The fracture morphology of the axial specimens was found to be independent of the matrix composition. Both the CPMg and the ZE41A axial specimens failed in a flat manner at approximately 90° to the stress axis with the failure propagating across fibers. The off-axis behavior was highly composition dependent, however. Failure of the 22.5° ZE41A specimens was similar to that of the axial specimens. The fracture surface was quite flat, oriented at 90° to the tensile axis, and fracture occurred through the fibers. In direct contrast, the off-axis CPMg specimens failed along the fiber/matrix interface.

Fatigue Behavior

The results of fatigue tests performed on CPMg and ZE41A in both 0 and 22.5° orientations are presented in Figure 2. When loaded axially the fatigue resistance of ZE41A was considerably lower than that of CPMg. However, al-

though both materials showed a marked reduction in fatigue resistance when loaded off-axis (22.5°), the degree of reduction was far less for ZE41A than for CPMg. Thus at 22.5° ZE41A was more resistant to fatigue than CPMg. This behavior is similar to the UTS dependence on alloy content and fiber orientation. The S-N curves for ZE41A exhibited slightly steeper slopes than the corresponding curves for CPMg. Thus the endurance limit, 10^6 cycles to failure, for ZE41A was approximately 0.62 UTS for both 0° and 22.5° while CPMg had an endurance limit of approximately 0.68 UTS at 22.5° and 0.78 UTS at 0°.

The axial CPMg and ZE41A specimens exhibited similar fracture morphologies. In both, fracture occurred across the fibers at an angle of approximately 90° to the tensile axis. The fracture morphology of the off-axis specimens was affected by the matrix composition, however. The 22.5° CPMg specimens failed parallel to the fiber axis with a significant difference between the fatigue and overload morphologies. The overload regions, Figure 3a, failed by decohesion of the fiber/matrix interface while fatigue cracking, Figure 3b, occurred along the direction of the fiber axis by a combination of crystallographic matrix cracking and delamination of the fiber/matrix interface. The 22.5° ZE41A specimens, on the other hand, failed across the fibers at around 90° to the tensile axis in both fatigue and overload, Figure 4, in the same manner as the axial specimens.

The similarity in the appearance of the fatigue and overload regions of the 0° and 22.5° ZE41A specimens and the 0° CPMg specimens made it impossible to determine the extent of fatigue cracking. River markings on the fracture surface did identify fatigue crack initiation sites, however. In both CPMg and ZE41A fatigue cracks initiated at process defects, usually large clumps of Al_2O_3 grains. These defects were not involved in initiation in the 22.5° CPMg

specimens. Examination of mating fracture surfaces in CPMg specimens indicated that failure occurred along the defect/matrix interface. Energy dispersive X-ray spectra taken from the mating surfaces always showed aluminum (Al_2O_3) on one surface and primarily magnesium on the other, confirming that fracture was along the interface. The mating fracture surfaces in ZE41A indicated that failure occurred through the defect rather than along its interface. Thus, although the initiation sites were similar the failure modes of the defects changed with matrix composition.

Auger Spectroscopy

The in-situ fracture of both CPMg and ZE41A occurred along fiber/matrix interfaces, making it possible to examine the composition of both troughs and fiber surfaces. Microscopic examination of the fiber surfaces in the Scanning Auger microprobe indicated that the fibers in CPMg, Figure 5, were covered with fine, almost continuous particles while the fibers in ZE41A, Figure 6, were covered with coarser and more discrete particles.

Spectra taken from a fiber trough and the surface of a fiber in CPMg are presented in Figure 7. The spectra indicate the presence of magnesium and oxygen in both the trough and the fiber surface. No other elements were observed on either the trough or the fiber surface. Comparison of the fine structure of the magnesium peaks and the oxygen to magnesium peak height ratios with spectra taken from laboratory standards (5) indicates that the trough was metallic magnesium containing a small amount of oxygen, possibly from residual vacuum contamination, and that the fiber surface was an oxide of magnesium, most likely MgO.

Spectra from a fiber trough and the surface of a fiber in ZE41A are presented in Figure 8. As in the CPMg, the fine structure of the magnesium

peaks and the oxygen-to-magnesium peak height ratios indicate that the trough was metallic magnesium and the fiber surface was an oxide of magnesium. In addition to the magnesium and oxygen, small quantities of zinc and aluminum were also present in both locations. No evidence of the presence of zirconium or rare earths, the other alloying elements in ZE41A, was found on either the trough or the fiber surface. The small carbon peak observed in the trough spectra is probably due to contamination rather than the actual presence of carbon in the specimen. To determine if either the zinc or aluminum were segregated at the fiber/matrix interface ion sputtering of the fracture surface was performed. No decrease in the zinc or aluminum signals was observed during sputtering, rather a slight increase was observed, Figure 8b. The oxygen peak decreased and the carbon peak, which was believed to be due to contamination, quickly disappeared during sputtering. Thus, the zinc and aluminum were not segregated at the interface but rather uniformly distributed in the area of the interface.

Transmission Electron Microscopy

Confirming the Auger results, a thin, submicron, reaction zone was observed in the thin foils of both CPMg, Figure 9, and ZE41A, Figure 10. The reaction zone particles in CPMg were finer, 0.14 μm average diameter versus 0.24 μm average diameter in ZE41A, and more closely spaced than those in ZE41A, thus presenting a geometrically smoother matrix/reaction zone interface. In addition, the reaction zone in CPMg was approximately a factor of two thinner than the 2 μm thick reaction zone in ZE41A. A considerable variation in grain size was also observed in the Al_2O_3 fibers.

The reaction zone precipitates were identified as MgO by microdiffraction. Typical microdiffraction patterns, (110) zone axis, are presented in

Figures 9 and 10. In both CPMg and ZE41A the particles were cubic with lattice parameters of 0.4230 and 0.4210 nm, respectively. These values are within measurement error of the published MgO lattice parameter of 0.4213 nm (6).

DISCUSSION

The properties of a composite material are determined by a combination of the fiber, matrix, and interfacial properties. In general, axial strength, both static and cyclic, is primarily dependent on the fiber volume fraction and the fiber strength. Matrix strength plays only a secondary role. On the other hand, transverse strength is more heavily influenced by the matrix and interfacial strengths. At intermediate angles the component controlling failure is controlled by the relative magnitudes of the shear and normal stresses that each component experiences as well as the individual strengths of each component. In general, matrix alloy additions can affect all three of the parameters that control composite behavior, i.e., fiber, matrix, and interfacial properties.

Although the microstructural state of the ZE41A matrix material is uncertain,* it is still possible to discuss, in terms of upper and lower limits, the effect of the alloy additions on matrix strength. In the fully solutionized condition substantial solid solution strengthening would be provided by the zinc. This lower limit case would provide a considerable improvement in matrix strength compared to CPMg. The zinc additions can also lead to

---

*It was not possible to define the microstructural state because data on the cooling rates employed during casting were not available. Further, the ion milling procedure employed in foil preparation could heat the foils slightly thus altering the matrix precipitate morphology.

precipitation hardening through the formation of Guinier-Preston zones, MgZn' precipitates, or MgZn precipitates (7,8). The formation of Mg_7Zn_3 is also possible (9). The presence of any of these precipitates would further strengthen the matrix. The presence of zirconium, which acts as a grain refiner in magnesium castings, is probably responsible for the slightly smaller grain size of the ZE41A. However, since the grain sizes of ZE41A and CPMg were both much larger than the fiber spacing it is doubtful that grain size has any significant bearing on mechanical properties. One might expect, therefore, that use of ZE41A rather than CPMg would result in a matrix with a higher yield strength, ultimate tensile strength, and fatigue resistance.

Since ZE41A has a higher matrix strength than CPMg, the lower axial tensile strength of the ZE41A material indicates that the fiber strength of the ZE41A is degraded. Using the rule of mixtures and a UTS of 90 MPa for the CPMg matrix, the resultant strength of the Al_2O_3 fibers is 950 MPa. A similar calculation for ZE41A using 165 MPa as the matrix strength (10) yields a fiber strength of 770 MPa. This represents a 19% reduction in fiber strength. Since the same type of fiber, i.e., FP Al_2O_3, was used in both materials and the CPMg fiber strength of 950 MPa is near the bottom of the scatter band (11), it can be concluded that the reduced fiber strength of ZE41A is due to reaction with the matrix material.

The crossover of the UTS versus fiber orientation curves suggests that the matrix and/or interfacial strength of ZE41A is higher than CPMg. From the earlier discussion of the effect of alloy additions on matrix strength, it is obvious that the ZE41A material has a higher matrix strength than the CPMg material. The change in off-axis fracture morphology from interfacial failure in CPMg to flat fracture across fibers in ZE41A suggests that the ZE41A material also has a higher interfacial strength. The change in the fracture mode

of the process defects which act as fracture initiation sites from interfacial failure in CPMg to fracture through the defect in ZE41A also supports an increased interfacial strength in ZE41A.

The reaction product was identified as MgO in both materials by microdiffraction. The TEM observations also indicated that the reaction zone in ZE41A was thicker and made up of larger particles than in CPMg. Thermodynamic calculations indicate that the formation of MgO from Al_2O_3 and Mg is possible for matrix magnesium concentrations exceeding 4 to 8 pct. (12), a condition which both CPMg and ZE41A easily satisfy. Further, Levi et al (12) have observed the formation of both MgO and $MgAl_2O_4$ spinel on FP Al_2O_3 fibers in contact with an Al-8% Mg alloy. The formation of MgO has also been observed in Al_2O_3 scales on Al-Mg alloys (13). The above results and the findings of the present study disagree with an earlier identification of the FP Al_2O_3/ZE41A reaction product as $MgAl_2O_4$ (14), which was performed by x-ray analysis of bulk specimens. Although the presence of $MgAl_2O_4$ is apparent from the x-ray data, the use of bulk specimens in the study precludes any identification of its location. Energy dispersive x-ray analysis profiles taken across the fiber/matrix interface (14) are also inconclusive as to the nature of the reaction product since the spacial resolution of the analysis was larger than the 0.2 m reaction zone which is present in this material. The Auger results support the formation of MgO in the reaction zone and, further, indicate that interfacial failure in both materials occurs at the reaction zone/matrix interface as opposed to the reaction zone/fiber interface. In addition, the lack of any segregation at the reaction zone/matrix interface indicates that the alloying elements in ZE41A were not directly responsible for the increased interfacial strength. Hence, it can be concluded that the interfacial strengthening observed in ZE41A is due to an increase in the size of the reaction zone and/or a change in the size and spacing of the MgO crystals and not any change in the

chemical nature of the reaction zone. The increased reaction zone is also consistent with the degradation in fiber strength observed in ZE41A. A large fraction of the reduced fiber strength is believed to be due to the development of notches on the fiber surfaces, induced by uneven chemical attack on the fibers during precipitation and growth of the MgO particles, since the actual reduction in Al_2O_3 cross section brought about by the formation of MgO accounts only for a small portion of the observed reduction. This explanation is consistent with observations in other composite systems (15-17).

The TEM and Auger results indicate that the matrix alloying elements are not incorporated in the reaction zone to any significant degree. Hence, the only plausible explanation for the differences observed in the sizes of the reaction zones between CPMg and ZE41A would be an inherent difference in processing. Liquidus temperatures, liquid metal infiltration temperatures and cooling rates were similar for the two alloys (18,19). A major difference exists in the solidification behavior, however. CPMg should undergo nearly congruent solidification while ZE41A experiences a large "mushy" zone due to the 120°C difference between its liquidus and solidus temperatures (18). It is postulated, therefore, that the larger reaction zone in ZE41A results from a longer contact time with more highly reactive liquid matrix. Experiments to test this hypothesis are presently underway.

To summarize the discussion to this point, the matrix alloy additions result directly in an increased matrix strength and indirectly in an increased interfacial strength and a decreased fiber strength. These results, which are consistent with the differences in tensile behavior between CPMg and ZE41A, can also be used to explain the differences in fatigue behavior between the two materials. Under axial loading the fibers bear most of the load and present the primary barrier to fatigue. Thus the reduction in fiber strength through an increased reaction zone observed in ZE41A would be expected to yield reduced

fatigue resistance. The lower interfacial strength in CPMg may also contribute to CPMg's higher fatigue resistance (20).

For one to understand the differences in off-axis fatigue behavior between CPMg and ZE41A it is necessary to consider both the strength differences of the individual components and the mechanics involved in off-axis loading. For loading at 22.5° to the fiber matrix, the off-axis orientation employed in this study, a relatively high normal stress and a relatively low shear stress would exist in the fibers, while a crack propagating along the fiber direction either in the matrix or along the interface would experience a relatively low normal stress and a relatively high shear stress (21). Considering this and the earlier observation that fatigue crack propagation in CPMg oriented at 22.5° occurred by a combination of crystallographic cracking of the Mg matrix and interfacial failure, it can be concluded that shear failure of the matrix-interface combination is possible at lower applied stresses than is normal fracture of the fibers.

Although the ZE41A matrix is also susceptible to the same type of crystallographic cracking as the CPMg matrix (9,22), its fatigue resistance is substantially higher. In addition, the ZE41A composite has a higher interfacial strength, the other component which contributed to fatigue crack propagation in CPMg; and a lower fiber strength, the component which did not participate in failure in CPMg. By increasing the fatigue resistance of the two weaker components and, at the same time, decreasing the resistance of the strongest component, a point should be reached at which a transition in fracture mode to progressive fracture of fibers occurs. This is apparently what has taken place in the ZE41A material.

The fracture and fatigue behavior of ZE41A at misorientation angles greater than 22.5° can be postulated by once again considering the mechanics of off-axis loading. As the misorientation angle increases, the fibers

experience lower normal stresses and cracks oriented along the fiber direction, i.e., either matrix or interfacial cracks, experience higher normal stresses (21). Thus at some higher angle, a transition to matrix and/or interfacial failure along the fiber direction would be expected. Even so, the ZE41A material would still be expected to maintain a higher strength than CPMg due to its higher matrix and interfacial strengths. Hence the alloy additions present in ZE41A would be expected to increase the angle at which the transition in failure mode occurs and also increase the off-axis strength.

CONCLUSIONS

The following conclusions can be drawn from the results of the present investigation.

(1) The alloying elements in ZE41A result directly in an increased matrix strength and indirectly in an increased fiber/matrix interfacial strength and a decreased fiber strength when compared to CPMg.

(2) The increased matrix strength is due to solid solution strengthening and/or precipitation hardening.

(3) The increased interfacial strength is due to a larger reaction zone and larger particles and not to any segregation to or change in chemistry of the reaction zone. The reaction zone was made up of MgO in both CPMg and ZE41A and interfacial failure occurred along the reaction zone/matrix interface. Segregation to this interface was not observed.

(4) The decreased fiber strength, which was estimated to be approximately 20%, was the result of the increased reaction between the matrix and fibers.

(5) The changes in the component strengths for ZE41A outlined above yielded reduced axial and increased off-axis tensile and fatigue properties.

ACKNOWLEDGEMENTS

The authors are grateful for the support of this work by the Army Research Office under Contract No. DAAG29-81-K-0049. The assistance in thin foil preparation which Mr. H. G. Saldana provided is also gratefully acknowledged.

REFERENCES

1. W. R. Hoover: J. Comp. Mat., 1976, Vol. 10, p. 106.
2. K. M. Prewo and K. G. Kreider: J. Comp. Mat., 1972, Vol. 6, p. 338
3. W. R. Kreuger: E. I. DuPont de Nemours and Co., Wilmington, DE, Private Communication, September 1979.
4. W. D. Riecke: Optik, 1962, Vol. 19, p. 81.
5. L. E. Davis, N. C. MacDonald, P. W. Palmberg, G. E. Riach, and R. E. Weber: Handbook of Auger Electron Spectroscopy, 2nd. ed., pp. 39-41, Physical Electronic Industries, Eden Prairie, MN, 1976.
6. X-Ray Powder Data File, ASTM STP 48-J, J. V. Smith, ed., p. 581, American Society for Testing Materials, Philadelphia, PA, 1960.
7. J. B. Clark: Acta Met., 1965, Vol. 13, p. 1281.
8. G. Mima and Y. Tanaka: Jap. Inst. Met., 1971, Vol. 12, p. 71.
9. A. K. Bhambra and T. Z. Kattamis: Met. Trans., 1971, Vol. 2, p. 1869.
10. J. Nunes: Report No. AMMRC SP 83-3, Army Materials and Mechanics Research Center, Watertown, Mass., April 1983.
11. R. T. Pepper and D. C. Nelson: Report No. NASA CR-167999, NASA-Lewis Research Center, Cleveland, OH, September 1982.
12. C. G. Levi, G. J. Abbaschian, and R. Mehrabian: Met. Trans.A, 1978, Vol. 9A, p. 697.
13. A. J. Brock and M. A. Heine: J. Electrochem. Soc., 1972, Vol. 119, p. 1124.
14. E. Chin: Report No. AMMRC SP 83-3, Army Materials and Mechanics Research Center, Watertown, Mass., April 1983.

15. D. W. Petrasek and J. W. Weeton, Trans. TMS-AIME, 1964, Vol. 230, p. 977.

16. A. G. Metcalfe, J. Compos. Mater., 1967, Vol. 1, p. 356.

17. A. Pattnaik and A. Lawley, Met. Trans., 1974, Vol. 5, p. 111.

18. ASM Metals Handbook, 9th ed., Volume 2 - Properties and Selection: Nonferous Alloys and Pure Metals, American Society for Metals, 1979, p. 523.

19. J. Widrig, E. I. Dupont de Nemours and Co., Wilmington, DE, Private Communication, October 1983.

20. M. Gouda, K. M. Prewo, and A. J. McEvily: Fatigue of Fibrous Composite Materials, ASTM STP 723, K. N. Lauraitis, ed., pp. 101-115, American Society for Testing Materials, Philadelphia, PA, 1981.

21. C. C. Chamis and J. H. Sinclair: Report No. NASA TN D-8215, NASA Lewis Research Center, Cleveland, OH, April 1976.

22. M. J. May and R. W. K. Honeycombe: J. Inst. Metals, 1963-64, Vol. 92, p. 41.

TABLE I

MECHANICAL PROPERTIES OF 55 V/O
Al_2O_3 FIBER REINFORCED MAGNESIUM

Specimen	Matrix Material	Orientation, deg.	YS, MPa	UTS, MPa	E, GPa
CP-0-A	CPMg	0		399*	192
CP-0-B	CPMg	0	321	567	202
CP-22-A	CPMg	22.5	30	192	153
CP-22-B	CPMg	22.5	23	199	157
ZE-0-A	ZE41A	0	-	488	186
ZE-0-B	ZE41A	0	-	504	184
ZE-0-C	ZE41A	0	487	496	-
ZE-0-D	ZE41A	0	406	406	-
ZE-22-A	ZE41A	22.5	-	393	157
ZE-22-B	ZE41A	22.5	-	379	155
ZE-22-C	ZE41A	22.5	325	406	-
ZE-22-D	ZE41A	22.5	325	388	-

* The UTS of specimen CP-0-A was reduced well below typical values by the presence of an unusually large process defect. This is discussed more fully in Part I.

LIST OF FIGURE CAPTIONS

Figure 1. Effect of fiber orientation on ultimate tensile strength for both commercially pure magnesium and ZE41A matrix materials.

Figure 2. Effect of fiber orientation and matrix alloy addition on the fatigue behavior of Al_2O_3 fiber-reinforced magnesium.

Figure 3. Scanning electron micrographs of typical overload (a) and fatigue (b) failures in off-axis CPMg specimens. Note that the failure in overload occurs almost exclusively along fiber/matrix interfaces while subcritical fatigue crack growth occurs primarily through the matrix.

Figure 4. Scanning electron micrographs illustrating typical fracture morphology (a) far from the initiation site, considered the overload region, and (b) adjacent to the initiation site, considered the fatigue region in off-axis ZE41A specimens. Although there is more evidence of ductility tearing in the overload region, failure in both regions occurs across the fibers rather than parallel to the fiber/matrix interface.

Figure 5. Scanning electron micrograph of a CPMg specimen fractured in the scanning Auger microprobe. A high magnification view of the fiber surface in Area 1 is shown in (b).

Figure 6. Scanning electron micrograph of a ZE41A specimen fractured in the scanning Auger microprobe. A high magnification view of the fiber surface in Area 2 is shown in (b).

Figure 7. Auger electron spectra taken from the fiber trough (a) and the fiber surface (b) of a CPMg sample which was fractured in situ.

Figure 8. Auger electron spectra taken from the fiber trough before (a) and after (b) sputtering and from the fiber surface (c) of a ZE41A sample which was fractured in situ.

Figure 9. Transmission electron micrograph of the fiber/matrix reaction zone in CPMg (a) and a diffraction pattern taken from a typical reaction zone particle (110 Zone) (b). The various constituents are indicated by: MG (CPMg matrix); RZ (reaction zone product); and FP (Al_2O_3 fiber).

Figure 10. Transmission electron micrograph of the fiber/matrix reaction zone in ZE41A (a) and a diffraction pattern taken from a typical reaction zone particle (110 Zone) (b). The various constituents are indicated by: MG (ZE41A matrix); RZ (reaction zone product); and FP (Al_2O_3 fiber).

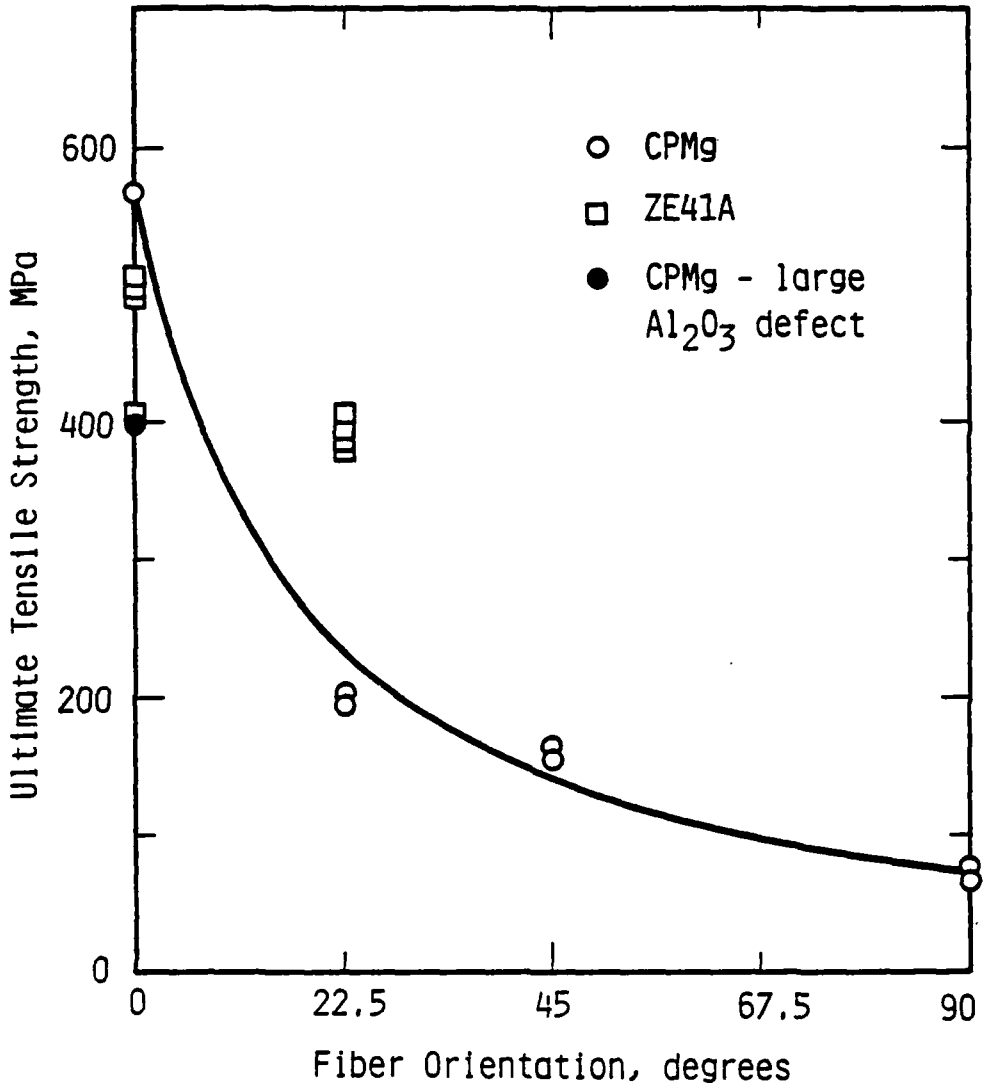

Figure 1. Effect of fiber orientation on ultimate tensile strength for both commercially pure magnesium and ZE41A matrix materials.

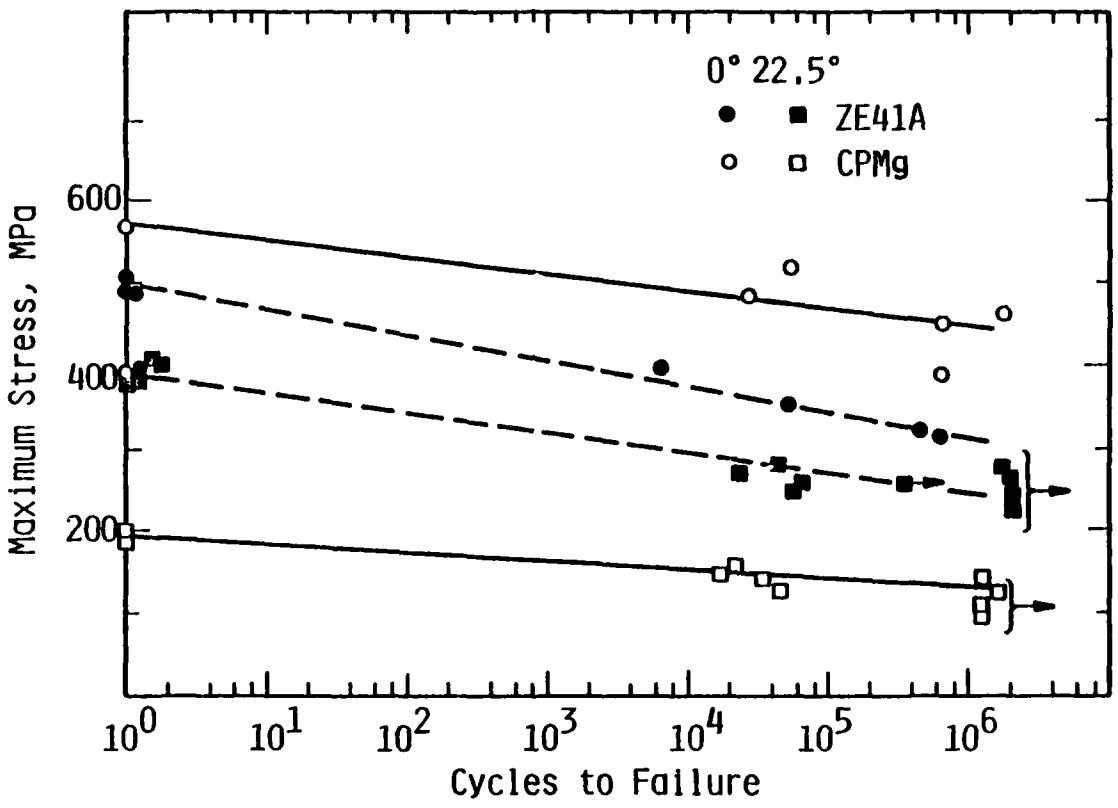

Figure 2. Effect of fiber orientation and matrix alloy addition on the fatigue behavior of Al_2O_3 fiber-reinforced magnesium.

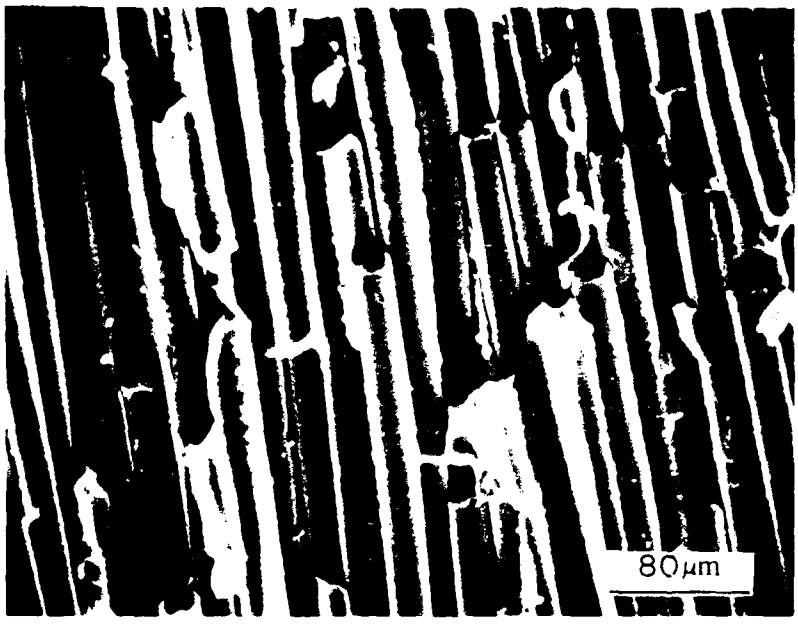

(a)

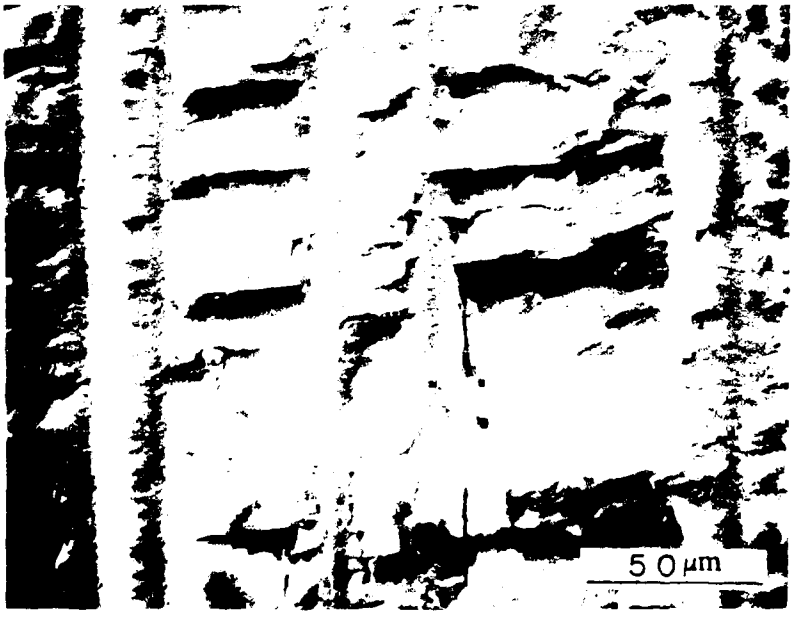

(b)

Figure 3. Scanning electron micrographs of typical overload (a) and fatigue (b) failures in off-axis CPMg specimens. Note that the failure in overload occurs almost exclusively along fiber/matrix interfaces while subcritical fatigue crack growth occurs parallel to the interfaces but primarily through the matrix.

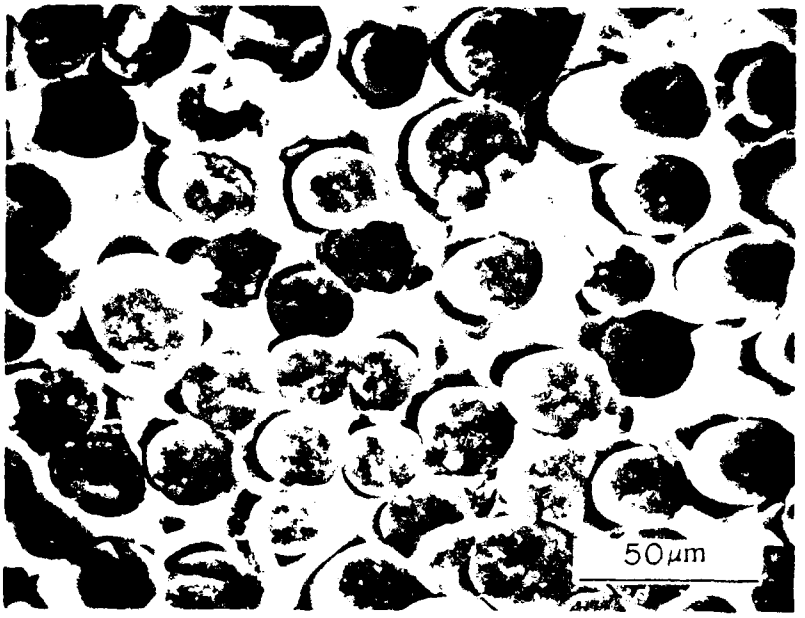

(a)

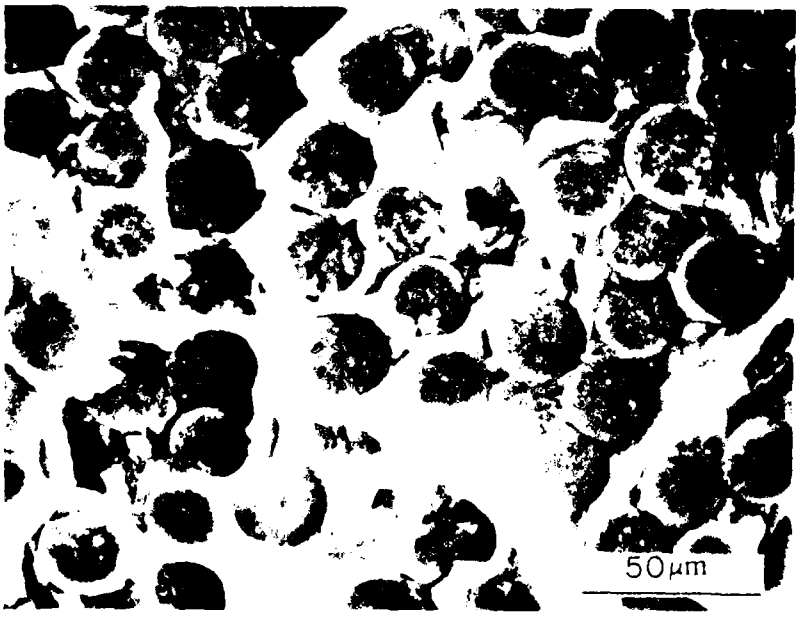

(b)

Figure 4. Scanning electron micrographs illustrating typical fracture morphology (a) far from the initiation site, considered the overload region, and (b) adjacent to the initiation site, considered the fatigue region in off-axis ZE41A specimens. Although there is more evidence of ductile tearing in the overload region, failure in both regions occurs across the fibers rather than along or parallel to the fiber/matrix interfaces.

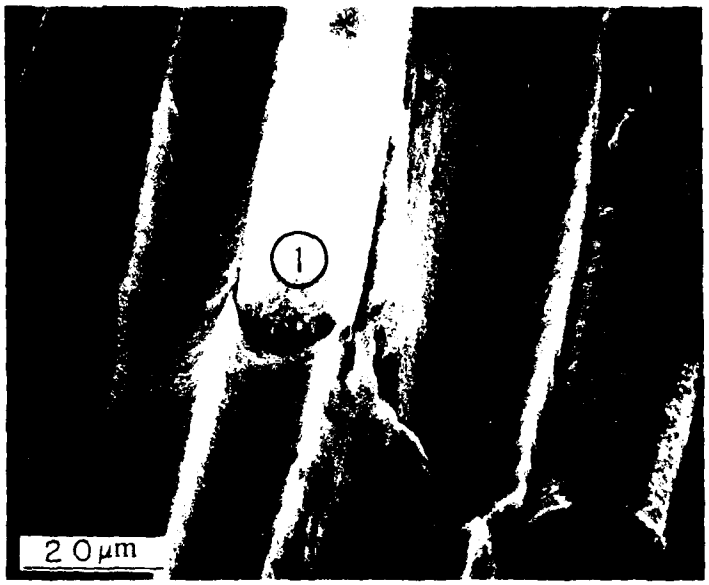

(a)

(b)

Figure 5. Scanning electron micrograph of a CPMg specimen fractured in the scanning Auger microprobe. A high magnification view of the fiber surface in Area 1 is shown in (b).

(a)

(b)

Figure 6. Scanning electron micrograph of a ZE41A specimen fractured in the Scanning Auger microprobe. A high magnification view of the fiber surface in Area 2 is shown in (b).

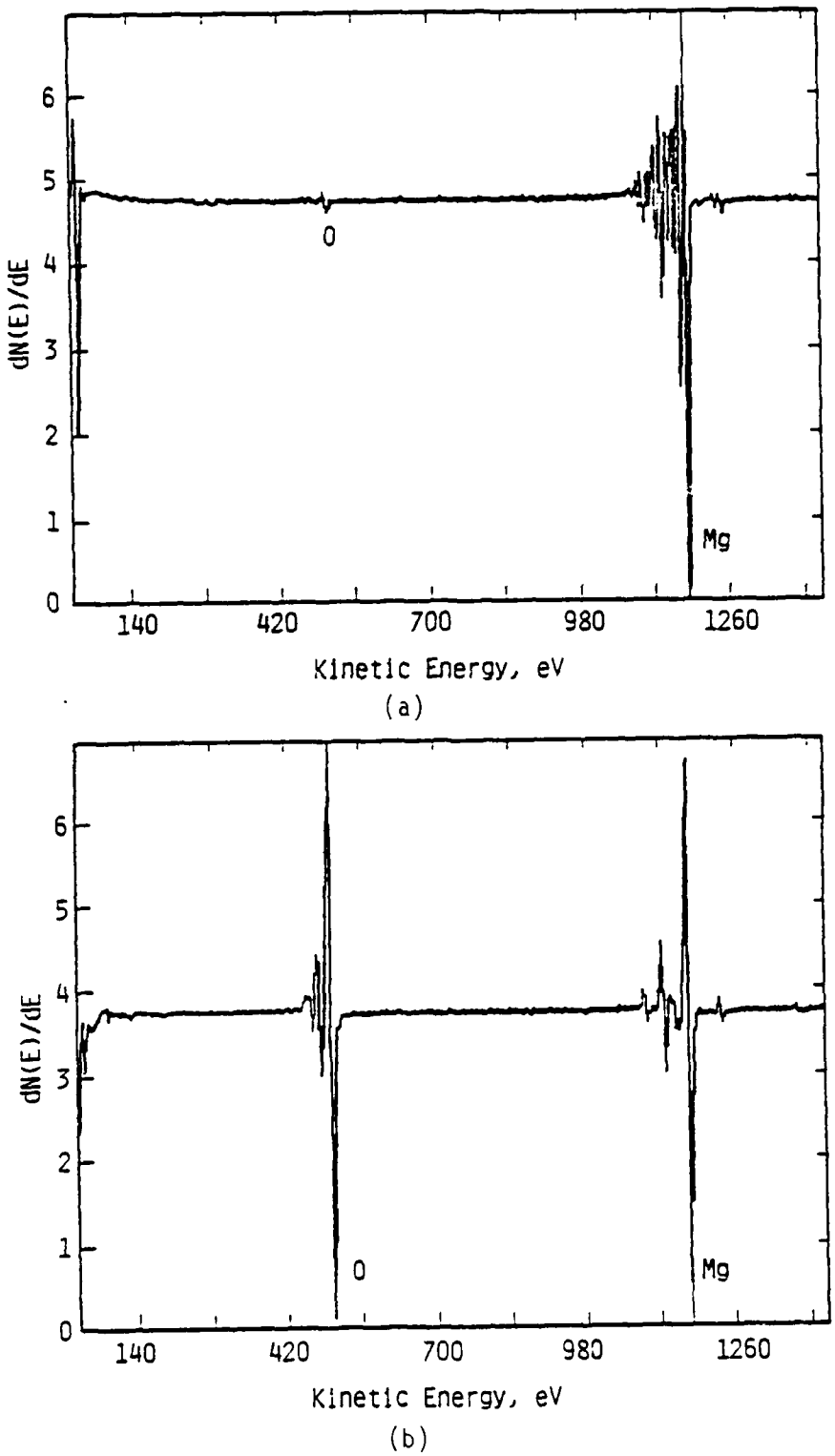

Figure 7. Auger electron spectra taken from the fiber trough (a) and the fiber surface (b) of a CPMg sample which was fractured in situ.

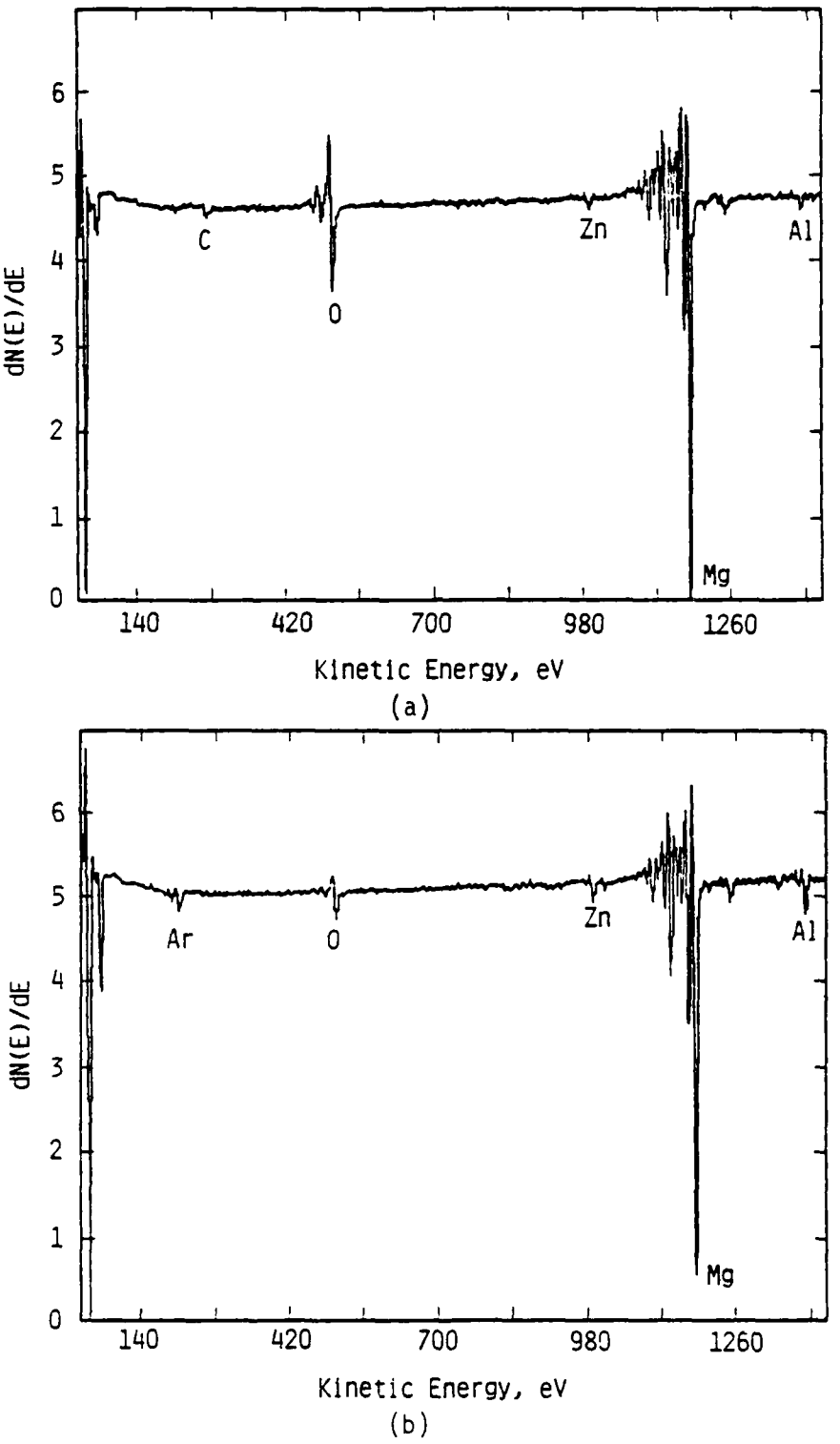

Figure 8. Auger electron spectra taken from the fiber trough before (a) and after (b) sputtering and from the fiber surface (c) of a ZE41A sample which was fractured in situ.

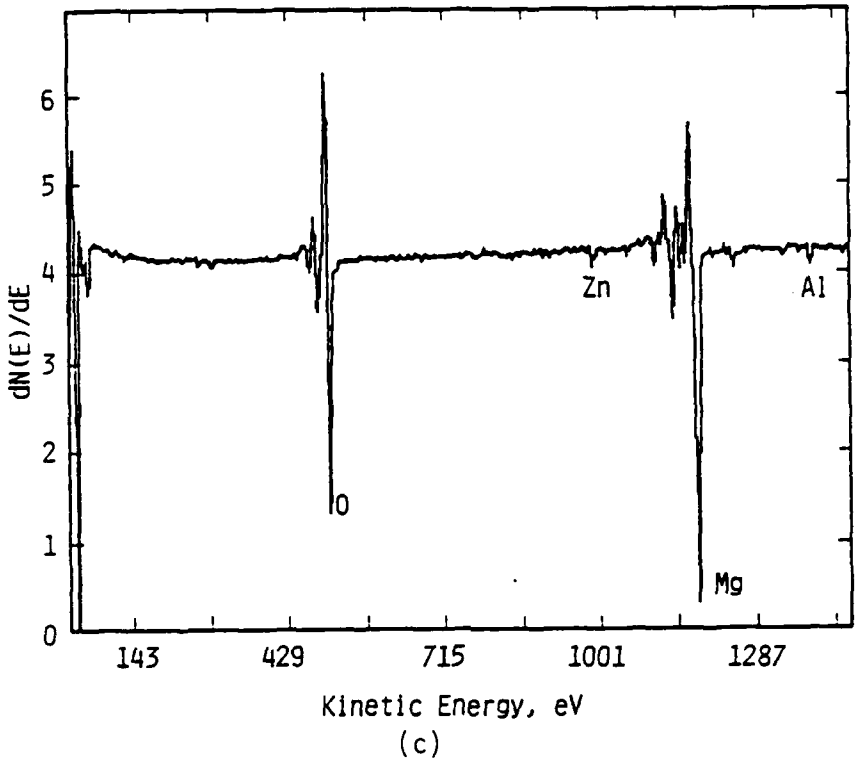

Figure 8 (Continued). Auger electron spectra taken from the fiber trough before (a) and after (b) sputtering and from the fiber surface (c) of a ZE41A sample which was fractured in situ.

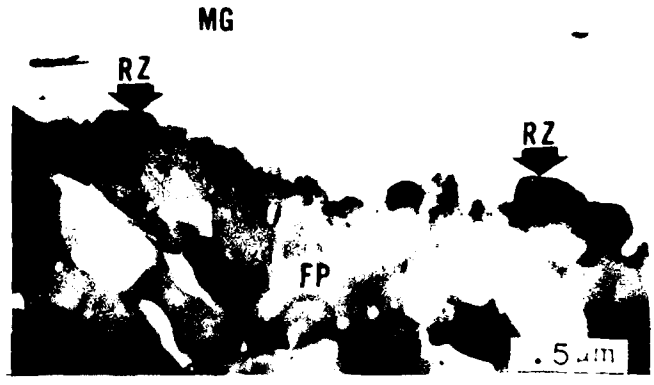

(a)

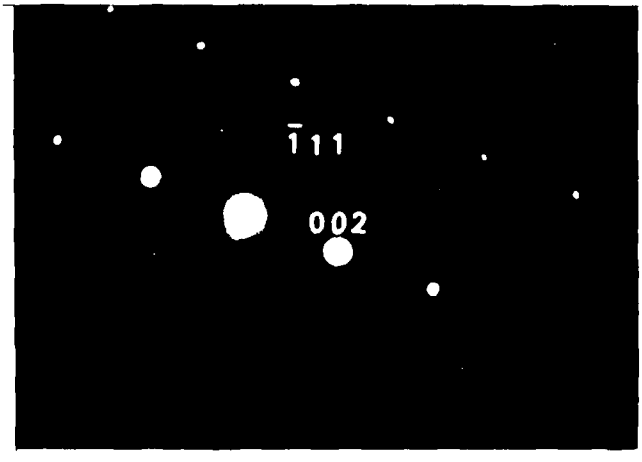

(b)

Figure 9. Transmission electron micrograph of the fiber/matrix reaction zone in CPMg (a) and a diffraction pattern taken from a typical reaction zone particle (110 Zone) (b). The various constituents are indicated by: MG (CPMg matrix); RZ (reaction zone product); and FP (Al_2O_3 fiber).

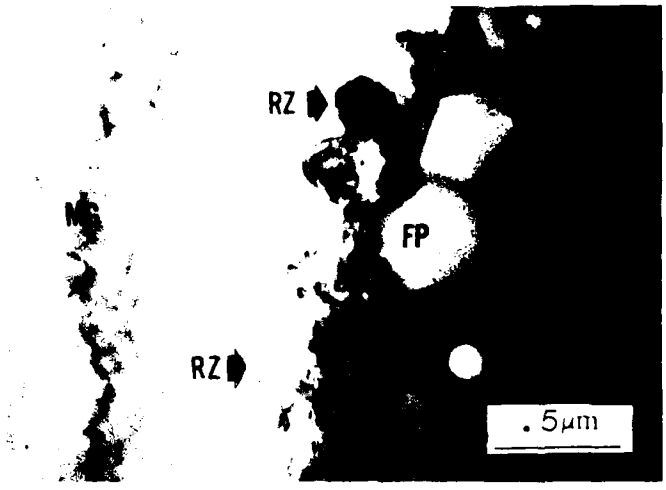

(a)

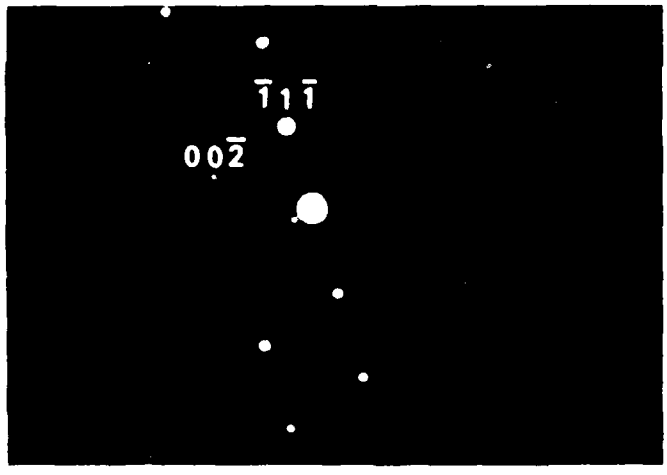

(b)

Figure 10. Transmission electron micrograph of the fiber/matrix reaction zone in ZE41A (a) and a diffraction pattern taken from a typical reaction zone particle (110 Zone) (b). The various constituents are indicated by: MG (ZE41A matrix); RZ (reaction zone product); and FP (Al_2O_3 fiber).

APPENDIX C

"CRITICAL STRESS INTENSITY FOR OFF-AXIS FRACTURE OF
Al_2O_3 FIBER REINFORCED MAGNESIUM"
BY K. S. CHAN, J. E. HACK AND R. A. PAGE
PUBLISHED IN METALLURGICAL TRANSACTIONS A,
VOLUME 15A, APRIL 1984

CRITICAL STRESS INTENSITY FOR OFF-AXIS FRACTURE OF Al_2O_3 FIBER REINFORCED MAGNESIUM

K. S. Chan, J. E. Hack, and R. A. Page

Southwest Research Institute
6220 Culebra Road
San Antonio, Texas 78284
USA

While studying the fracture behavior of fiber-reinforced composite materials a number of investigators (1-6) have concluded that K_c, the critical stress intensity factor, is a material parameter and as such should be useful for design purposes. These studies have also established that, despite the obvious inhomogeneities, linear elastic fracture mechanics can be directly applied to orthotropic composite materials if the following conditions are satisfied: (i) the orientation of the flaw coincides with one of the principal directions of elastic symmetry; and (ii) crack advance occurs in a self-similar manner (5,6). To be a successful design parameters, however, K_c, as calculated by linear elastic fracture mechanics, LEFM, techniques, must be geometry independent. Although K_c has been shown to be independent of crack length in metal matrix composites (1-3), Barnby and Spencer (7) have shown that compliance solutions derived for an elastic continuum may not adequately predict the compliance dependence on crack length in fiber-reinforced polymers. The latter result raises questions about the geometry independence of K_c when applied to orthotropic materials. In this study, the off-axis fracture behavior of a unidirectional Al_2O_3 fiber-reinforced magnesium composite was investigated. As will be discussed later, overload fracture of these composites is predominantly along fiber-matrix interfaces. Such a fracture path satisfies both the elastic symmetry and the similitude requirements. LEFM solutions were thus utilized to calculate stress intensity factors for a variety of measured crack geometries and orientations.

The Al_2O_3 fiber-reinforced magnesium specimens were produced by E. I. duPont de Nemours and Co. with continuous unidirectional Al_2O_3 fibers of 20 μm average diameter in a commercially pure magnesium matrix. Fiber

contents of 35 and 55 v/o were included in the test matrix. Rectangular samples, 1.27 cm x 0.25 cm x 15.2 cm long, were machined with the fibers lying in the plane of the 0.25 cm x 15.2 cm face and oriented at 22.5, 45, and 90° to the tensile axis.

Fatigue tests were performed to failure at a frequency of 10 Hz, an R-ratio of 0.1, and a series of maximum stresses ranging from 50 MPa to 200 MPa. Failure occurred along the fiber direction in both the fatigue and overload regions. Overload failure was primarily along fiber-matrix interfaces, Figure 1a, while fatigue cracking was primarily through the magnesium matrix, Fiber 1b. Because of this change in fracture morphology it was possible to determine the dimensions of the fatigue crack at the time of failure.

Figure 2 illustrates the configuration of the cracked composite specimens subjected to a remotely applied tensile stress, σ. The crack is aligned parallel to the reinforcing fibers but both the crack and the fibers are inclined at an angle, θ, to the stress axis. The normal stress, $\sigma_{y'y'}$, and the shear stress, $\sigma_{x'y'}$, acting on the crack plane are given as:

$$\sigma_{y'y'} = \sigma \sin^2 \theta \qquad [1]$$

and

$$\tau_{x'y'} = \sigma \sin \theta \cos \theta$$

The cracked composite is therefore subjected to either Mode I (in-plane opening) or mixed Mode I and Mode III (out-of-plane sliding) loadings. For unidirectional composites the stress intensity factors associated with the combined normal and shear stresses are (8):

$$K_I = \beta_1 \sigma_{y'y'} \sqrt{\pi a} = \beta_1 \sigma \sin^2 \theta \sqrt{\pi a}$$

$$K_{III} = \beta_3 \tau_{x'y'} \sqrt{\pi a} = \beta_3 \sigma \cos \theta \sin \theta \sqrt{\pi a} \qquad [2]$$

where β_1 and β_3 are the geometry correction factors for Mode I and Mode III cracks, respectively, and a is the crack length measured in the plane of the crack.

The crack geometries observed in the composite tended to have complex shapes. Quite a few of them were, however, of well-defined fracture mechanics geometries. These include single and double edge cracks, corner cracks, and eccentric center cracks. Figure 3 summarizes these crack geometries (Figure 3a-d) and gives examples of some of the irregularly shaped cracks also observed in the composite (Figure 3e-f). For the edge cracks and the eccentric center crack, β_1 corresponds to the finite-width correction factor and was obtained from references 9 and 10, respectively. β_1 for the corner crack was obtained from reference 11 and it includes the front face, back face, finite-width, and flaw shape correction factors. The values for β_3 are obtained from reference 12; the same finite-width correction factors are applicable for Mode III loadings of single edge, double edge and center cracks. In the case of corner cracks, the β_1 used in computing the Mode I stress intensity was also used to compute the Mode III stress intensity.

For computational purposes, the irregularly shaped cracks were idealized as either edge cracks or eccentric center cracks, as illustrated in Figure 3e and f. The lengths of the "equivalent" through-thickness cracks were computed from the actual cracked area, A_{CR}, on the basis of equality of areas between the through-thickness and the actual irregularly shaped cracks. Using this equivalent cracked area method, the length of the equivalent through-thickness crack was computed from A_{CR} as:

$$a_e = \frac{A_{CR}}{t} \quad \text{for an edge crack} \qquad [3]$$

and $$a_e = \frac{A_{CR}}{2t} \quad \text{for a center crack}$$

After obtaining a_e, the geometry correction factor and the stress intensity factor were calculated using the procedures described earlier. A summary of the fracture stress, crack lengths, geometry correction factors and the computed stress intensity factors is shown in Table I.

The values of K_{Ic} and K_{IIIc} at which unstable fracture occurred were computed by substituting the maximum applied stress into Eq. [2]. As the crack path is predominantly along fiber-matrix interfaces, the calculated K_{Ic} and K_{IIIc} represent the critical Mode I and Mode III stress intensities on the fiber-matrix interface and are thus reasonable measures of the resistance of the interface against normal and shear stress fracture, respectively. The effective stress intensity associated with the mixed-mode fracture was obtained by summing the Mode I and Mode III strain energy release rate components. For orthotropic materials with transverse isotropy (13)

$$K_{eff} = \sqrt{K_I^2 + K_{III}^2 \left(\frac{E_T}{2\mu_L}\right)} = (E_T G)^{1/2} \qquad [4]$$

where μ_L and E_T are the shear and Young's elastic moduli in the longitudinal and transverse directions, respectively, and G is the total strain energy release rate.

Figures 4a and 4b illustrate that both the K_{Ic} and K_{eff} values are slightly dependent on the crack angle. Thus, it is concluded that off-axis fracture of the composites does not obey a critical K_{Ic} or K_{eff} criterion. The relative role of normal stress and shear stress in the fracture of fiber-matrix interfaces is illustrated in Figure 5 which indicates that both the K_I and K_{III} components are important. For mixed Mode I and III loading the fracture criterion can be generalized as (5,6)

$$\left(\frac{K_I}{K_{Ic}}\right)^m + \left(\frac{K_{III}}{K_{IIIc}}\right)^n = 1 \qquad [5]$$

where K_{Ic} and K_{IIIc} are the critical stress intensity factors for pure Mode I and Mode III fracture, respectively. In an isotropic material, m and n are both two. Failure of orthotropic materials has been found to obey Eq. [5] with m = n = 2 (5,14) or m = 1 and n = 2 (4,6). From Figure 5, K_{Ic} is approximately 4.5 MPa$\sqrt{m}$ and the K_{IIIc} value appears to be similar to the K_{Ic}. Using K_{IIIc} = 5 MPa$\sqrt{m}$ and m = n = 2, Eq. [5] has been found to fit the experimental data adequately, as illustrated in Figure 5. In contrast, a critical strain energy release rate criterion (computed from Eq. [4]) underestimates the K_c values of the composites (see Figure 5).

In summary, the results indicate that the off-axis fracture of Al_2O_3 fiber-reinforced commercially pure magnesium appears to be controlled by both the normal and shear stress components acting on the fiber-matrix interface. In addition, similar K_{Ic} and K_{IIIc} values were determined for a variety of crack geometries, indicating that K_c is indeed geometry independent for the case of interfacial delamination at fairly low stresses. Thus K_c should be effective both as a design parameter and as an indicator

of relative interfacial strengths, provided that the different modes of cracking are taken into account and the basic fracture mechanics assumption of similitude is not violated.

Acknowledgement

The authors are grateful for the support of this work by the Army Research Office under Contract No. DAAG29-81-K-0049.

REFERENCES

1. J. R. Hancock and G. D. Swanson: Composite Materials: Testing and Design, ASTM STP 497, pp. 299-310, 1972.
2. W. R. Hoover and R. E. Allred: Proceedings of the Dynamic Crack Propagation Symposium, G. C. Sih, ed., pp. 613-622, Noordhoff International, Leyden, England, 1973.
3. W. R. Hoover: J. Comp. Mat., 1976, vol. 10, p. 106.
4. B. Spencer and J. T. Barnby: J. Mater. Sci., 1976, vol. 11, p. 83.
5. E. M. Wu: Composite Materials Workshop, S. W. Tsai, J. C. Halpin, and N. J. Pagano, eds., p. 20, Technomic Publishing, Standford, CT, 1968.
6. E. M. Wu: Trans. ASME, 1967, vol. E34, p. 967.
7. J. T. Barnby and B. Spencer: J. Mater. Sci., 1976, vol. 11, p. 78.
8. T. S. Cook and C. A. Rau, Jr.: Prospect of Fracture Mechanics, G. C. Sih, H. C. VanElst and D. Broek, eds., p. 509, Noordhoff International, Leyden, England, 1974.
9. D. Broek: Elementary Engineering Fracture Mechanics, p. 76, Sijthoft and Noordhoff, The Netherlands, 1978.
10. M. Isida: ASME Trans., J. Appl. Mech., 1966, vol. 88, p. 674.
11. J. C. Newman, Jr.: NASA TN D-8244, 1976.
12. H. Tada, P. Paris, and G. Irwin: The Stress Analysis of Cracks Handbook, Del Research, PA, 1973.
13. G. C. Sih and H. Liebowitz: Fracture, H. Liebowitz ed., vol. II, p. 68, Academic Press, New York, 1968.
14. R. J. Sandford and S. R. Stonesifer: Report No. 7112, Naval Research Laboratory, Washington, D.C., 1970.

TABLE I

A SUMMARY OF FRACTURE MECHANICS DATA OF Al_2O_3 FIBER-REINFORCED Mg COMPOSITE INCLUDING CRACK GEOMETRY, CRACK LENGTH, GEOMETRY CORRECTION FACTORS, FRACTURE STRESS (σ), AND THE CRITICAL STRESS INTENSITY FACTORS

Specimen	Crack Geometry	Crack Length, mm	Geometry Correction Factors β_1	Geometry Correction Factors β_3	σ, MPa	K_{Ic}, MPa$\sqrt{m}$	K_{IIIc}, MPa$\sqrt{m}$
55*-22**-F1	b	2.48	1.14	1.07	138	1.95	4.52
55-22-F3	b	2.66	1.14	1.08	131	1.92	4.33
55-22-F4	a	2.18	1.31	1.05	145	2.20	3.96
55-22-F5	a	2.69	1.40	1.09	159	2.86	5.52
55-22-F8	c	1.65/2.42+	.70	1.03	255	2.22	4.49
55-22-F9	c	1.65/1.69+	.72	1.03	241	2.13	4.33
55-45-F2	a	1.70	1.24	1.03	97	4.36	3.63
55-45-F3	a	2.18	1.31	1.05	95	4.30	3.44
55-45-F4	a	2.30	1.34	1.06	100	5.69	4.50
55-45-F5	d	1.80	1.16	1.04	100	4.36	3.91
55-90-F1	c	1.45/2.42+	.85	--	62	3.60	--
55-90-F2	a	1.03	1.16	--	64	4.20	--
55-90-F3	a	0.85	1.15	--	64	3.82	--
55-90-F4	a	1.57	1.22	--	63	5.44	--
55-90-F5	d	1.27	1.17	--	61	4.48	--
35-22-F1	a	1.81	1.25	1.04	145	1.92	3.95
35-22-F3	a	1.57	1.22	1.03	172	1.70	4.20
35-22-F4	a	1.69	1.23	1.03	152	1.91	4.73
35-22-F5	a	2.30	1.33	1.06	169	2.67	5.29
35-45-F2	d	1.51	1.10	1.02	71	2.68	2.49
35-45-F3	a	2.18	1.31	1.05	79	4.30	3.44
35-45-F4	b	2.06	1.14	1.05	73	3.35	3.08
35-45-F5	a	2.48	1.36	1.07	72	4.31	3.39
35-90-F1	d	0.65	1.00	--	83	3.74	--
35-90-F2	a	0.97	1.16	--	76	4.85	--
35-90-F3	d	1.12	1.04	--	69	4.26	--
35-90-F4	a	2.18	1.31	--	64	6.91	--
35-90-F5	d	0.94	1.10	--	62	3.70	--

*Volume fraction of fiber.

**The angle θ (in degree) between the crack and the applied stress σ.

+Crack depth.

a = edge crack.

b = double edge crack.

c = corner crack.

d = eccentric center crack.

LIST OF FIGURE CAPTIONS

Figure 1. Typical fracture morphology of off-axis specimens in overload failure (a) and fatigue failure (b).

Figure 2. Schematic of off-axis specimen indicating both the crack and the fibers make an angle θ with the applied stress σ. The coordinate system of the mixed Mode I and III crack is indicated by the x'-y' axes.

Figure 3. Crack geometries observed in the composite specimens.

Figure 4. K_{Ic} and K_{eff} versus crack angle for both 35 and 55 volume percent fiber.

Figure 5. Calculated Mode I stress intensity factor, K_I, versus calculated Mode III stress intensity factor, K_{III}, for both 35 and 55 volume percent fiber. Solid line is for $K_{Ic} = 4.5$ MPa$\sqrt{m}$ and $K_{IIIc} = 5$ MPa$\sqrt{m}$.

(a)

(b)

Figure 1. Typical fracture morphology of off-axis specimens in overload failure (a) and fatigue failure (b).

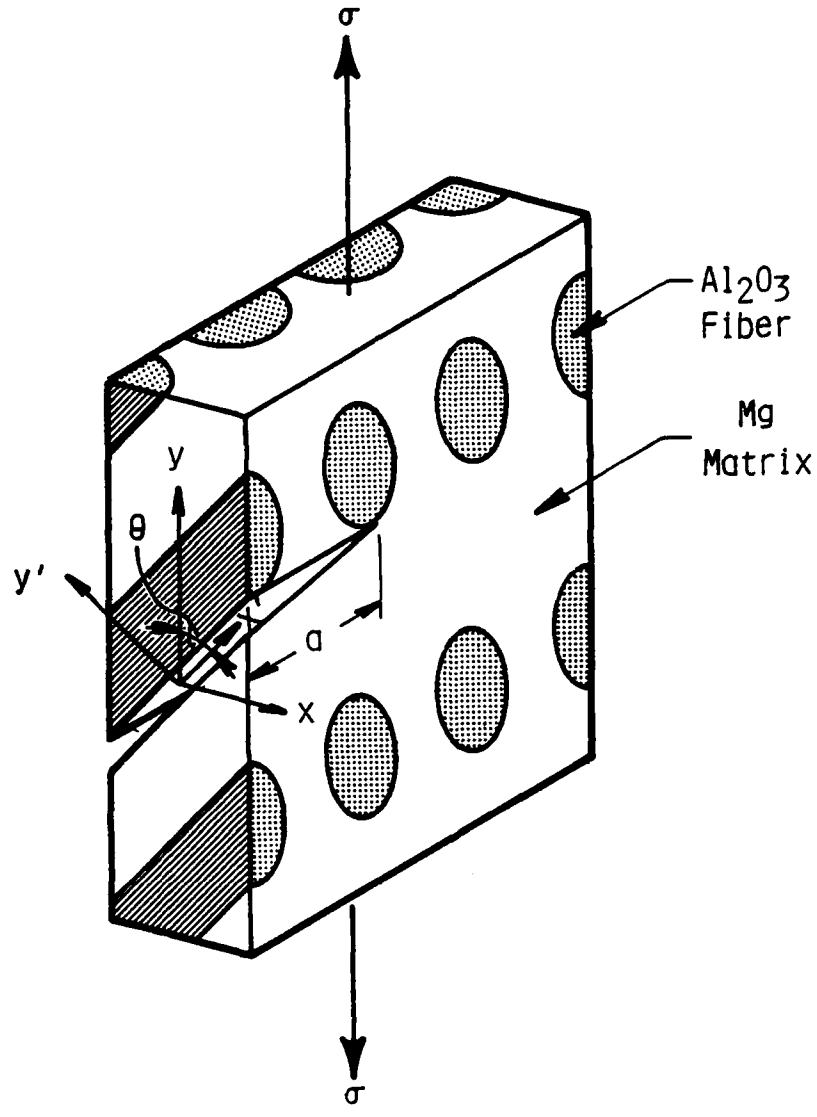

Figure 2. Schematic of off-axis specimen indicating both the crack and the fibers make an angle θ with the applied stress σ. The coordinate system of the mixed Mode I and III crack is indicated by the x'-y' axes.

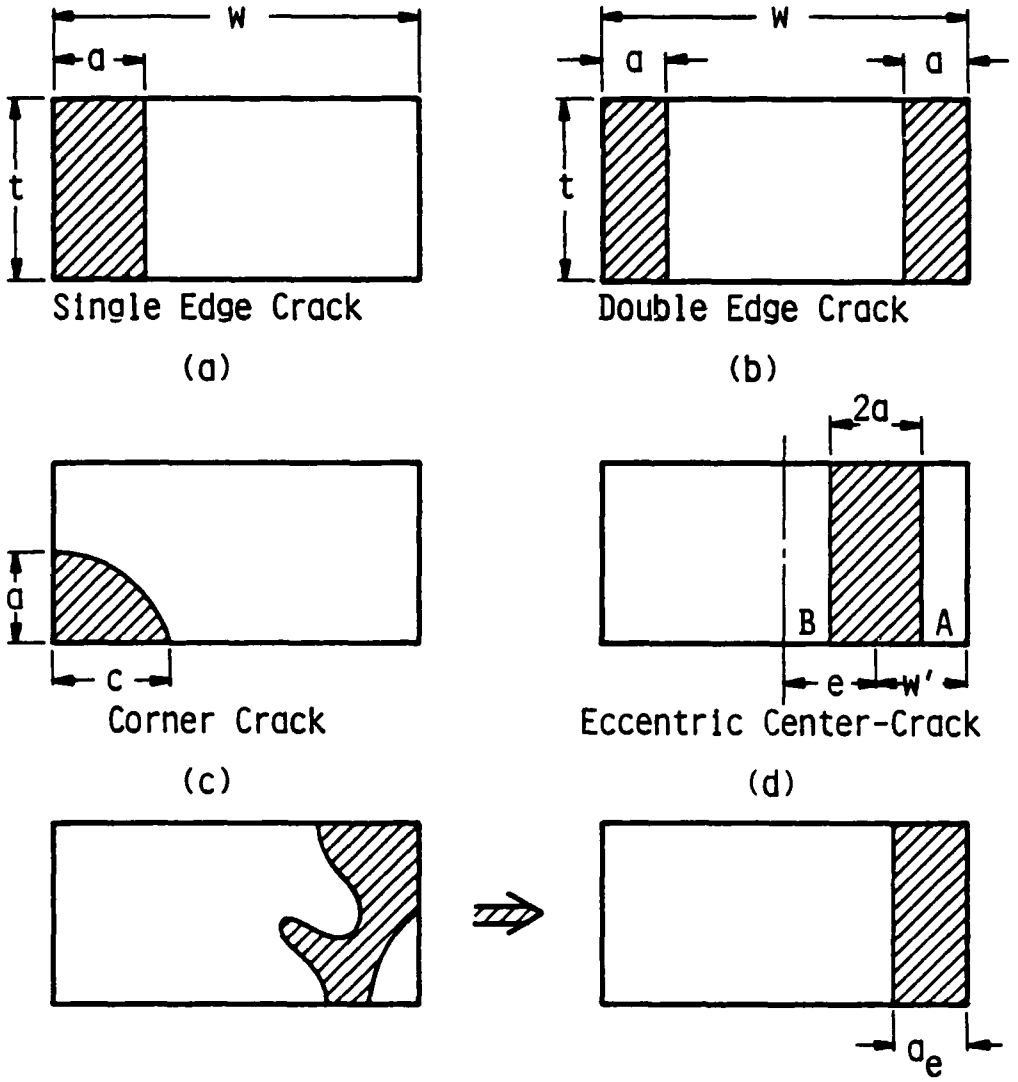

Figure 3. Crack geometries observed in the composite specimens.

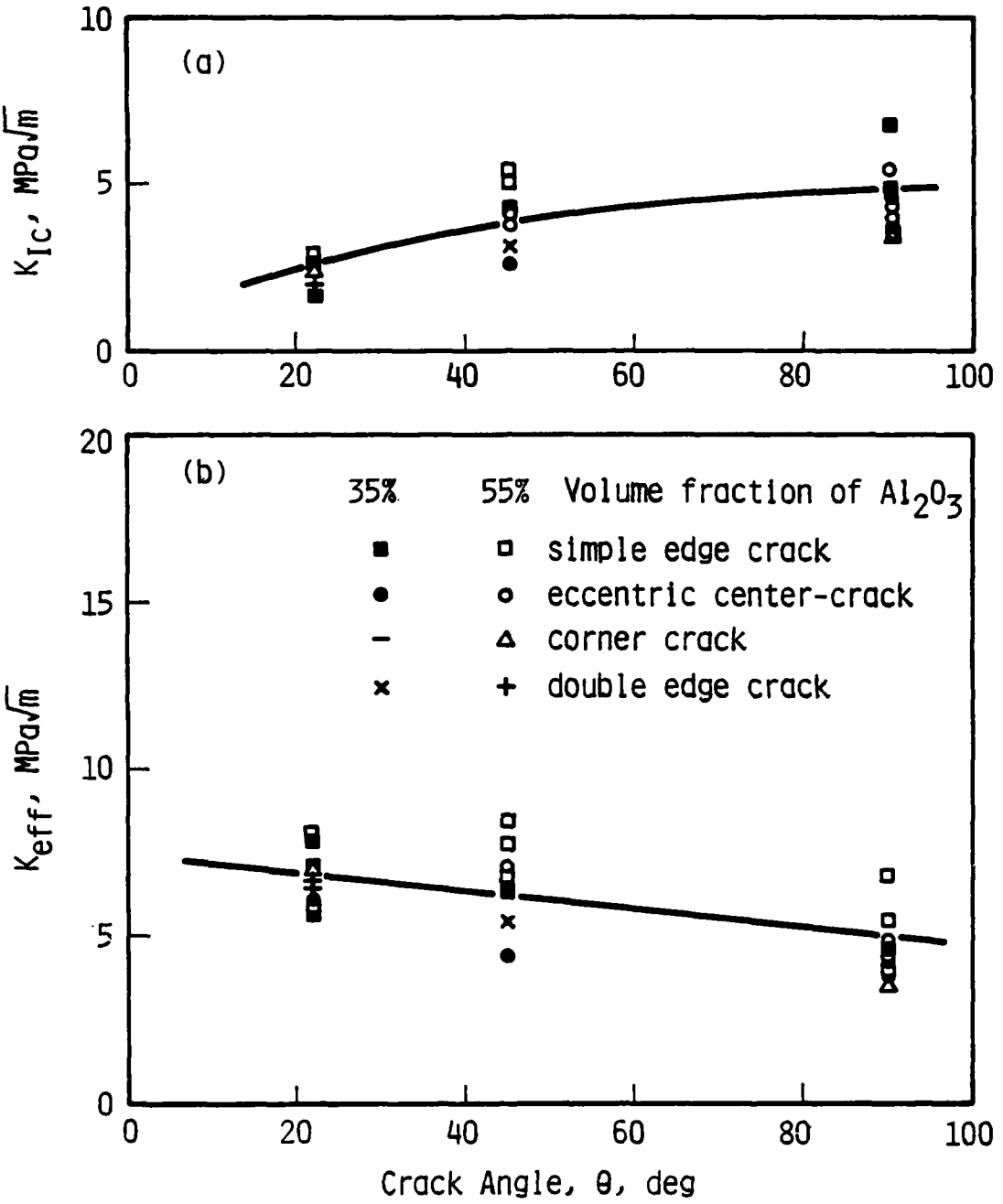

Figure 4. K_{Ic} and K_{eff} versus crack angle for both 35 and 55 volume percent fiber.

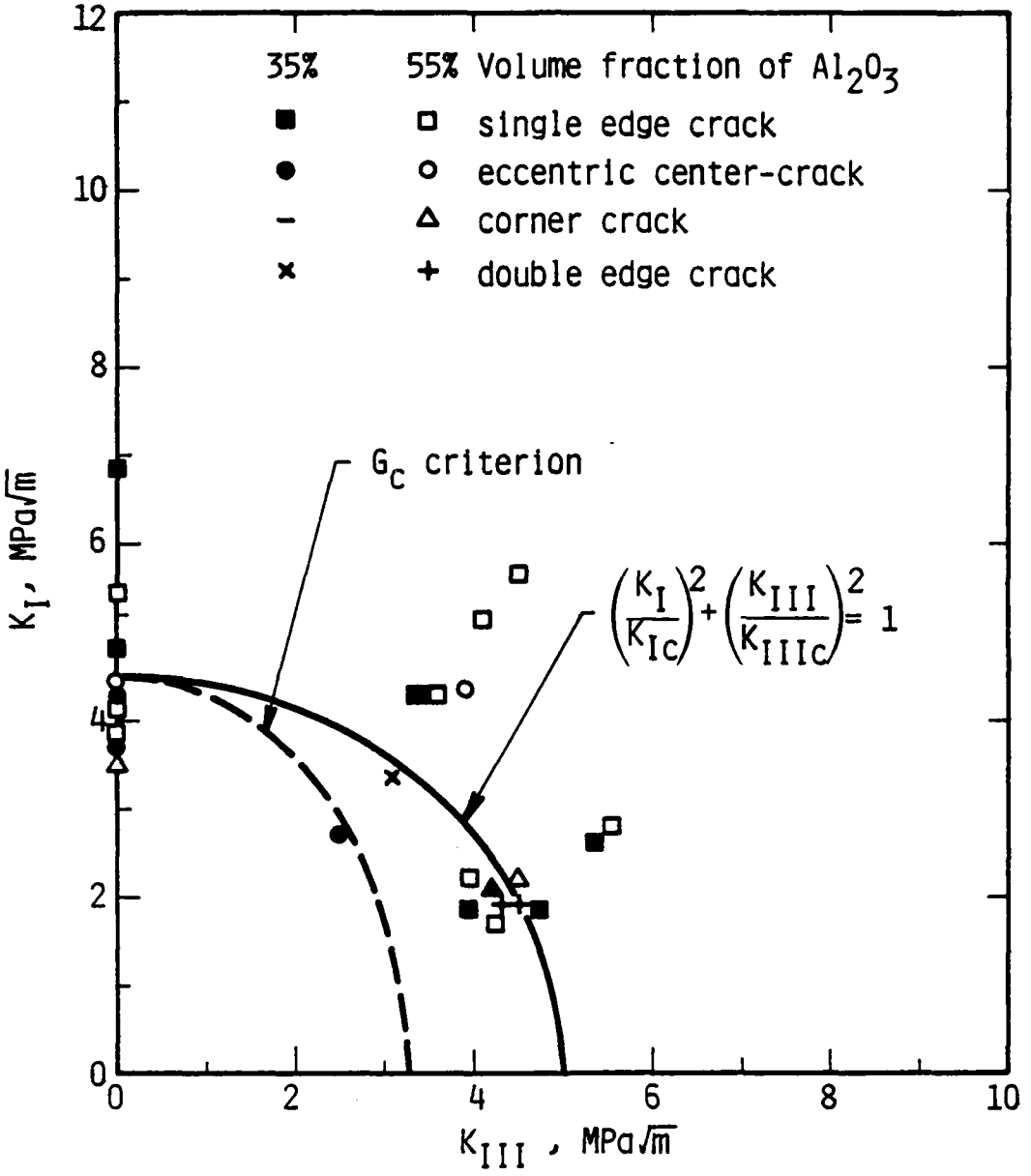

Figure 5. Calculated Mode I stress intensity factor, K_I, versus calculated Mode III stress intensity factor, K_{III}, for both 35 and 55 volume percent fiber. Solid line is for K_{Ic} = 4.5 MPa$\sqrt{m}$ and K_{IIIc} = 5 MPa$\sqrt{m}$.

APPENDIX D

"THE INFLUENCE OF THERMAL EXPOSURE ON INTERFACIAL REACTIONS AND STRENGTH IN ALUMINUM OXIDE FIBER REINFORCED MAGNESIUM ALLOY COMPOSITES"

BY J. E. HACK, R. A. PAGE AND R. SHERMAN

SUBMITTED FOR PUBLICATION TO
METALLURGICAL TRANSACTIONS A

THE INFLUENCE OF THERMAL EXPOSURE ON INTERFACIAL REACTIONS AND STRENGTH IN ALUMINUM OXIDE FIBER REINFORCED MAGNESIUM ALLOY COMPOSITES

by

J. E. Hack, R. A. Page and R. Sherman

Southwest Research Institute
Department of Materials Sciences
San Antonio, TX 78284

Matrix composition and heat treatment have been shown to influence off-axis properties in a number of metal-matrix composite systems (1,2). Recent studies of the fatigue and tensile behavior of unidirectional Al_2O_3 fiber reinforced composites with either a commercially pure magnesium (C.P.) or a ZE41A magnesium alloy (Mg-4.25Zn-0.5Zr-1.25RE) matrix revealed a dramatic shift in failure mode with a change in matrix composition (3,4). In the C.P. matrix material, it was found that off-axis fatigue and tensile properties were suppressed due to a combination of a low fiber/matrix interfacial strength and a soft matrix. The drastic drop in fatigue and tensile properties with increasing angle between the fibers and the stress axis was found to correspond with a change in failure mode from flat fracture across the fibers under axial loading conditions to interfacial and/or matrix failure along the fiber orientation for off-axis loading in all the orientations studied (3). The ZE41A composites, on the other hand, failed across the fibers in both axial and off-axis fatigue and tensile tests when the angle of misorientation between the stress axis and the fibers was less than 45° (4,5).

The difference in off-axis failure mode between the two materials was attributed to increases in interfacial and matrix strengths with a subsequent decrease in fiber strength in the ZE41A matrix composite. It

was also found that the alloying elements in ZE41A did not directly contribute to the improved interfacial strength. Interfacial reaction zone particles were identified by electron diffraction as MgO in both composites. Also, no segregation of impurity or alloying elements to the fiber/matrix interface region was observed with Auger Electron Spectroscopy (AES). The only difference observed between the interfacial reaction zones was that the MgO particles in the ZE41A matrix material were consistently about twice as large as those found in the C.P. matrix composites (4). Based on these results, it was felt that the difference in reaction zone size (and, therefore, mechanical properties) was due to inherent differences in processing.

Liquidus temperatures, liquid metal infiltration temperatures and cooling rates were found to be similar for the two materials (6,7). However, the manner in which the two matrix alloys solidify differs significantly. C.P. Mg should undergo nearly congruent solidification while ZE41A passes through a large "mushy zone" which arises from the 120°C difference between its liquidus and solidus temperatures (7). It was postulated that the larger reaction zone in ZE41A results from a longer contact time with the highly reactive liquid matrix.

In order to test this hypothesis, samples of C.P. matrix composites were heat treated above the melting point of the matrix (650°C) in an argon environment for various time and temperature combinations. Table I gives the details of the thermal exposures. The specimens were then fractured parallel to the fiber direction in-situ in a scanning Auger microprobe (SAM). Both fractography and AES analyses of exposed interfaces were performed in the SAM. In addition, thin foils were prepared by ion milling for examination by transmission electron microscopy.

TABLE I

THERMAL EXPOSURE PARAMETERS

Specimen	Exposure Temperature	Exposure Time
AR	--	--
TE1	675°C	15 min.
TE2	725°C	15 min.
TE3	725°C	30 min.

Low and high magnification fractographs of the as-received specimen (AR) and the specimen exposed at 725°C for 15 minutes (TE2) are presented in Figure 1. It can be seen from the fractographs that the fracture path in specimen AR was almost exclusively through the Mg/MgO interface, as discussed previously (4). The fracture surface in specimen TE2, however, showed a considerable amount of matrix failure. In particular, the high magnification views of the fiber surfaces (Figures 1b and 1d) revealed virtually no metal adhering to the fiber in specimen AR while dimpled rupture of Mg is visible on the exposed fiber surface in sample TE2. The amount of matrix failure observed generally increased with exposure time and temperature. These observations were corroborated by the AES data given in Figure 2. The fine structure of the magnesium peaks taken from a fiber trough (Figure 2a) and a fiber surface (Figure 2b) in as-received material are typical of metallic magnesium and MgO, respectively (8). Thus, failure in specimen AR occurred along the matrix/reaction zone interface with very little of the metallic matrix adhering to the reaction zone. As the degree of thermal exposure was increased, however, magnesium peaks in spectra taken from exposed fiber surfaces showed a gradual transition toward a fine structure typical of metallic magnesium (Figures 2c-e). This indicates a trend toward a greater amount of metallic Mg adhering to the MgO particles in the reaction zone as the reaction is allowed to proceed for a longer time. In other words, the fracture path was shifted from the Mg/MgO interface out into the matrix as the degree of thermal exposure increased.

Figure 3 contrasts the MgO particle sizes observed in specimens AR (Figure 3a) and TE2 (Figures 3b and 3c). These TEM micrographs clearly show an increase in MgO particle size* from an average of 0.14 μm in the as-received material to approximately 0.28 μm for specimen TE2. Combined with the fractography and AES results, these data, as well as the results reported in references (3) and (4), generally point to an increase in interfacial strength due to growth of the MgO reaction zone particles.

Thus, it appears that off-axis properties in Al_2O_3 fiber reinforced Mg are controlled by reaction zone thickness alone. Alloying elements which merely provide a lengthened liquid metal contact time by modification of the solidification behavior apparently do not directly affect the interfacial strength. Therefore, it may be possible to eliminate the need for such alloying elements by judicious process control during liquid metal infiltration. Experiments are planned to test this hypothesis by evaluating the influence of MgO particle size on the mechanical properties of C.P. matrix composites. It should be noted, however, that increases in interfacial strength induced by increased fiber/matrix reaction are generally accompanied by a decrease in fiber and, subsequently, composite axial properties. Eventually, alloying additions which are expected to directly modify reaction zone composition and structure may be a more attractive avenue to explore for improved composite properties.

---

*The Riecke (9) microdiffraction technique was used to identify the reaction zone particles as MgO in both materials.

AD-A143 003 A NEW APPROACH TO THE EVALUATION OF THE EFFECTS OF 2/2
STRESS STATE AND INTER..(U) SOUTHWEST RESEARCH INST SAN
ANTONIO TEX DEPT OF MATERIALS SCI.. J E HACK ET AL.
UNCLASSIFIED 31 MAY 84 ARO-17207.3-MS DAAG29-81-K-0049 F/G 11/4 NL

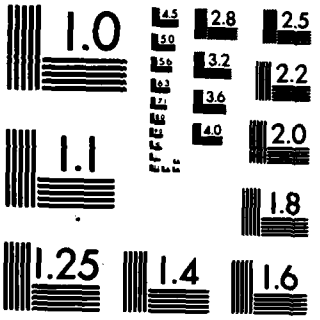

Acknowledgements

The authors are grateful for the support of this work by the Army Research Office under Contract No. DAAG29-81-K-0049. The assistance of Messrs. H. Saldana and K. Short in sample preparation and helpful discussions with G. R. Leverant are also greatly appreciated.

REFERENCES

1. W. R. Hoover: J. Comp. Mat., 1976, vol. 10, p. 106.
2. K. M. Prewo and K. G. Kreider: J. Comp. Mat., 1972, vol. 6, p. 338.
3. J. E. Hack, R. A. Page and G. R. Leverant, Met. Trans. A, in press.
4. R. A. Page, J. E. Hack, R. Sherman and G. R. Leverant, Met. Trans. A, in press.
5. J. E. Hack, R. A. Page, G. R. Leverant, unpublished research, Southwest Research Institute, San Antonio, TX, 1984.
6. J. Widrig, E. I. Dupont de NeMours and Co., Wilmington, DE, Private Communication, October 1983.
7. ASM Metals Handbook, 9th ed., Volume 2 - Properties and Selection: Nonferrous Alloys and Pure Metals, American Society for Metals, 1979, p. 523.
8. L. E. Davis, N. C. MacDonald, P. W. Palmberg, G. E. Riach and R. E. Weber: Handbook of Auger Electron Spectroscopy, 2nd ed., Physical Electronics Industries, Eden Prairie, MN, 1976, pp. 39-41.
9. W. D. Riecke, Optik, 1962, vol. 19, p. 81.

FIGURE CAPTIONS

Figure 1. Fractography of selected Al_2O_3 fiber reinforced C.P. Mg composite fracture in situ in the SAM.

(a) Overall fracture surface of as-received material.

(b) Fiber surface in as-received material.

(c) Overall fracture surface material held at 725°C for 15 minutes.

(d) Fiber surface in material held at 725°C for 15 minutes.

Figure 2. Expanded view of Mg peak in Auger electron spectra of fracture surfaces for all materials studied.

(a) Trough in as-received material.

(b) Fiber surface in as-received material.

(c) Fiber surface in material held at 675°C for 15 minutes.

(d) Fiber surface in material held at 725°C for 15 minutes.

(e) Fiber surface in material held at 725°C for 30 minutes.

Figure 3. Transmission electron micrographs of fiber/matrix interfacial region in selected materials. The various constituents are indicated by: MG (C.P. Mg matrix); RZ (Reaction Zone product); and FP (Al_2O_3 fiber).

(a) As-received material.

(b) Material held at 725°C for 15 minutes.

(c) Material held at 725°C for 15 minutes.

(a) Overall fracture surface of as-received material.

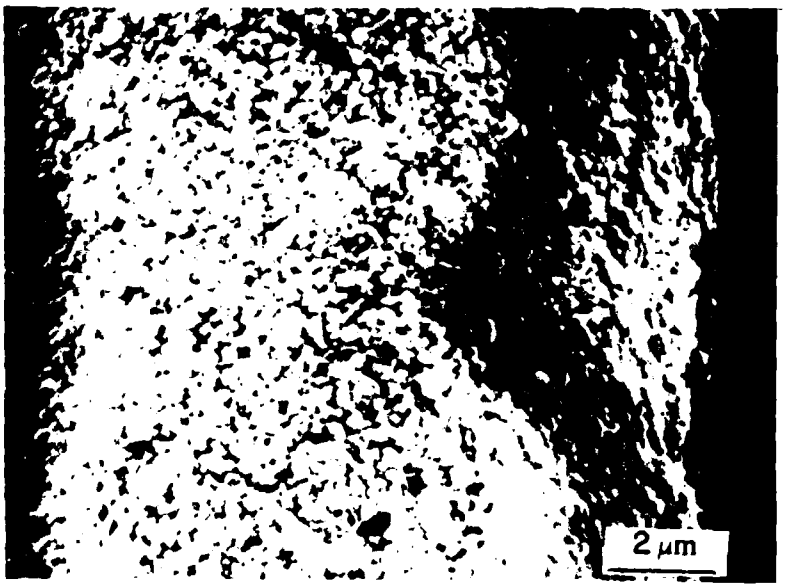

(b) Fiber surface in as-received material.

Figure 1. Fractography of selected Al_2O_3 fiber reinforced C.P. Mg composite fracture in situ in the SAM.

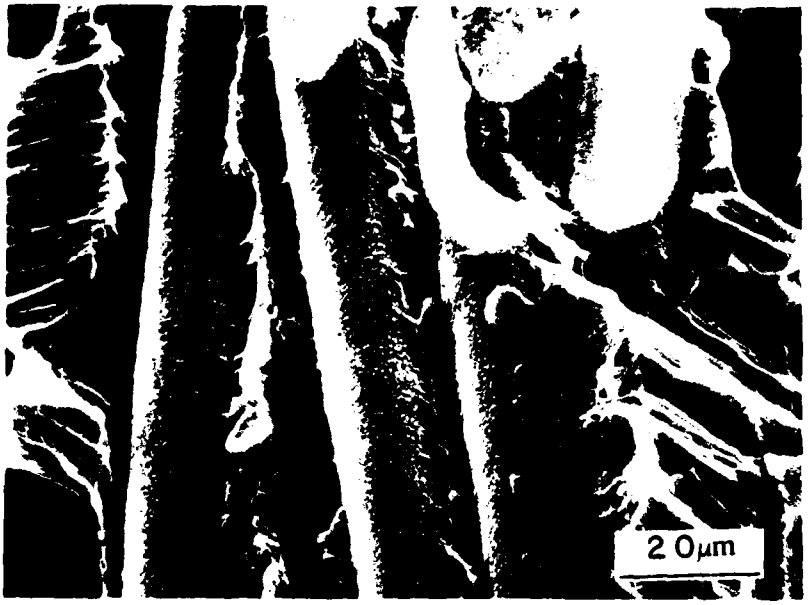

(c) Overall fracture surface of material held at 725°C for 15 minutes.

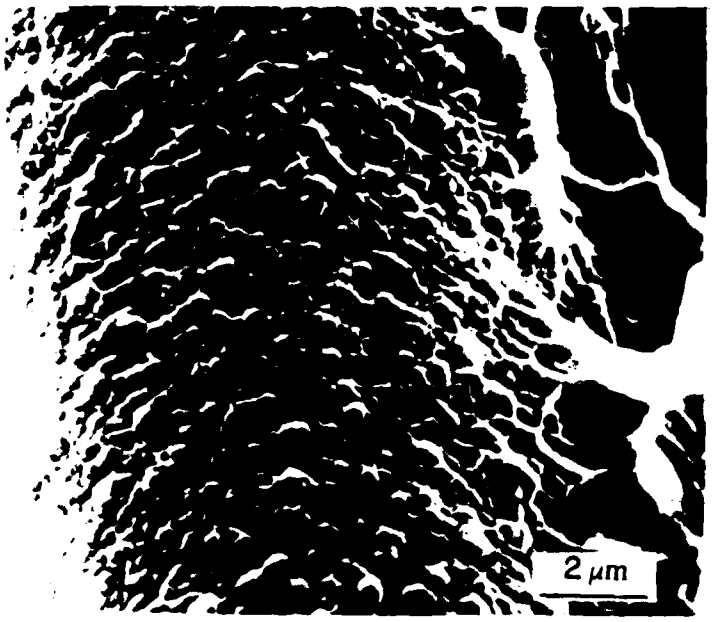

(d) Fiber surface in material held at 725°C for 15 minutes.

Figure 1 (continued). Fractography of selected Al_2O_3 fiber reinforced C.P. Mg composite fracture <u>in situ</u> in the SAM.

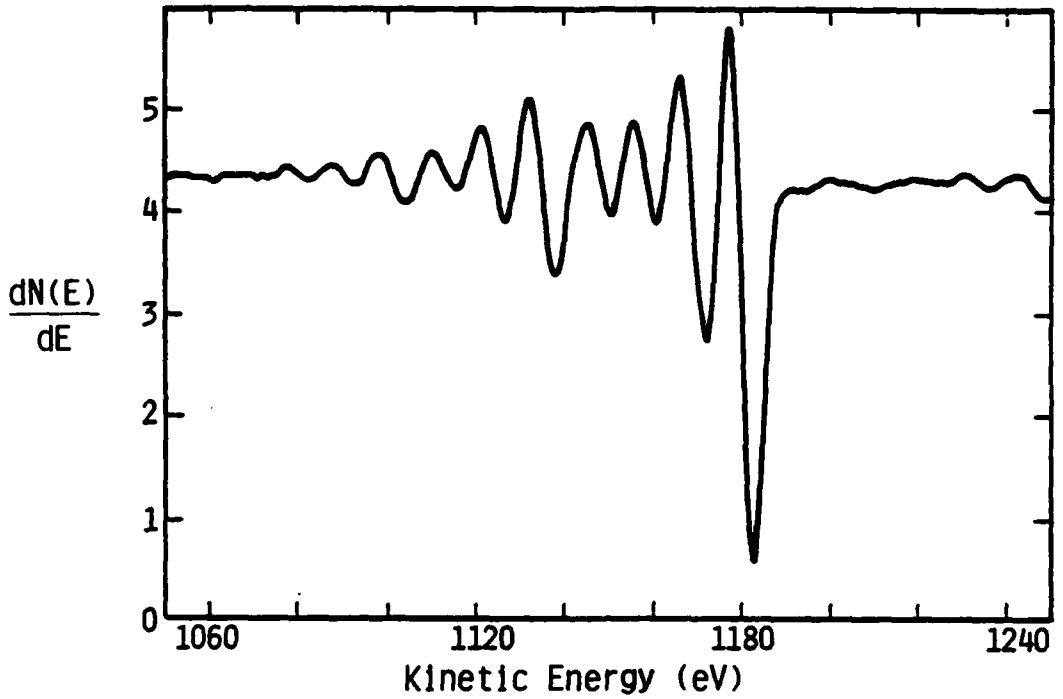

(a) Trough in as-received material.

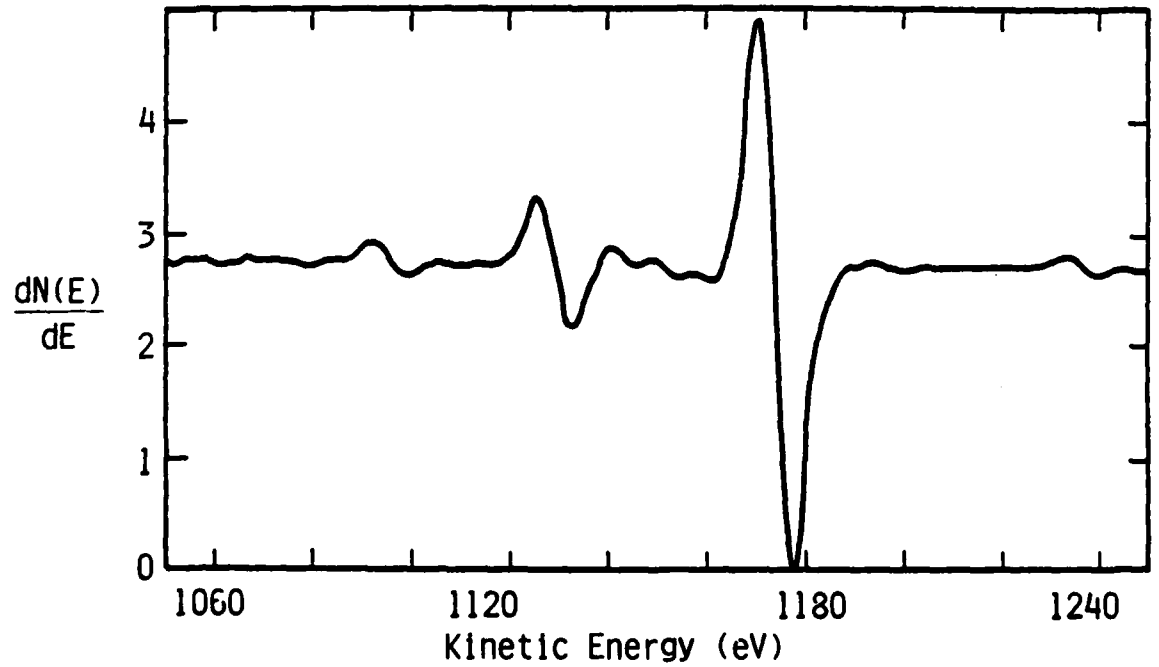

(b) Fiber surface in as-received material.

Figure 2. Expanded view of Mg peak in Auger electron spectra of fracture surfaces for all materials studied.

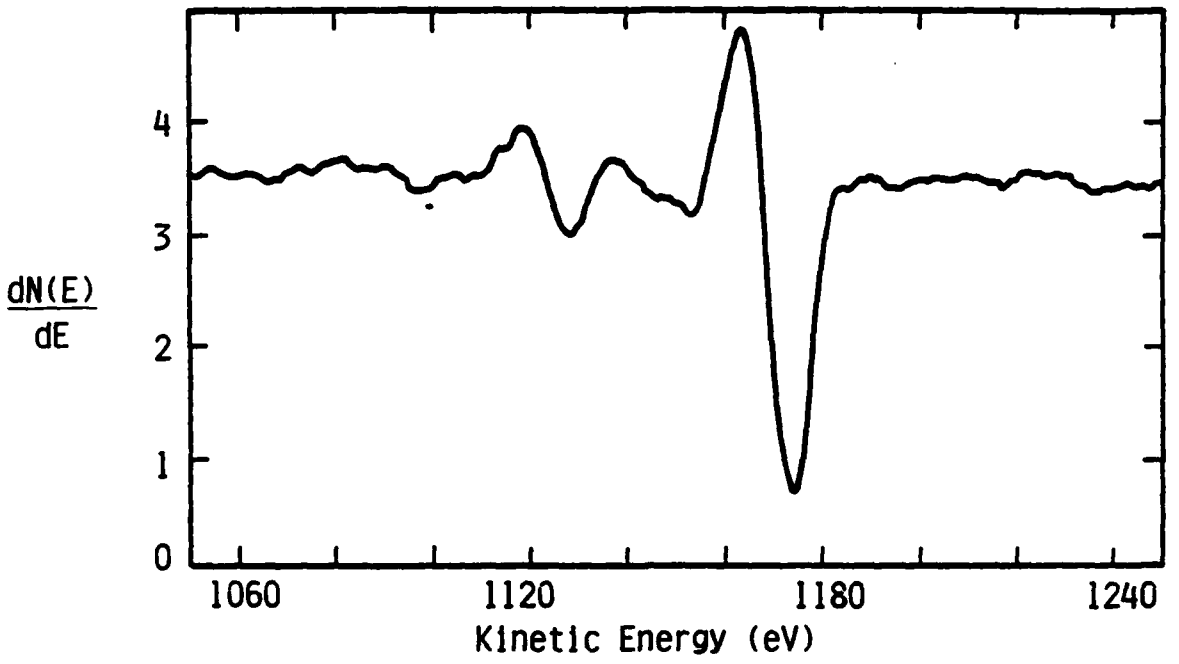

(c) Fiber surface in material held at 675°C for 15 minutes.

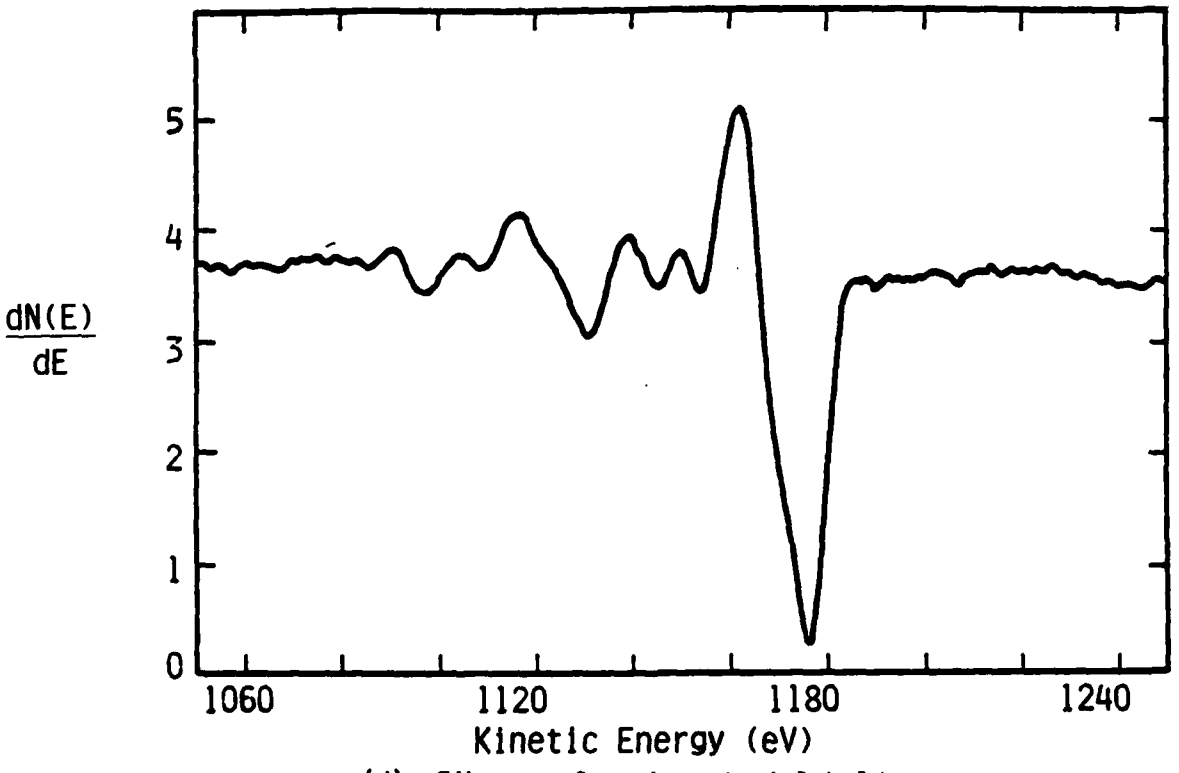

(d) Fiber surface in material held at 725°C for 15 minutes.

Figure 2 (continued). Expanded view of Mg peak in Auger electron spectra of fracture surfaces for all materials studied.

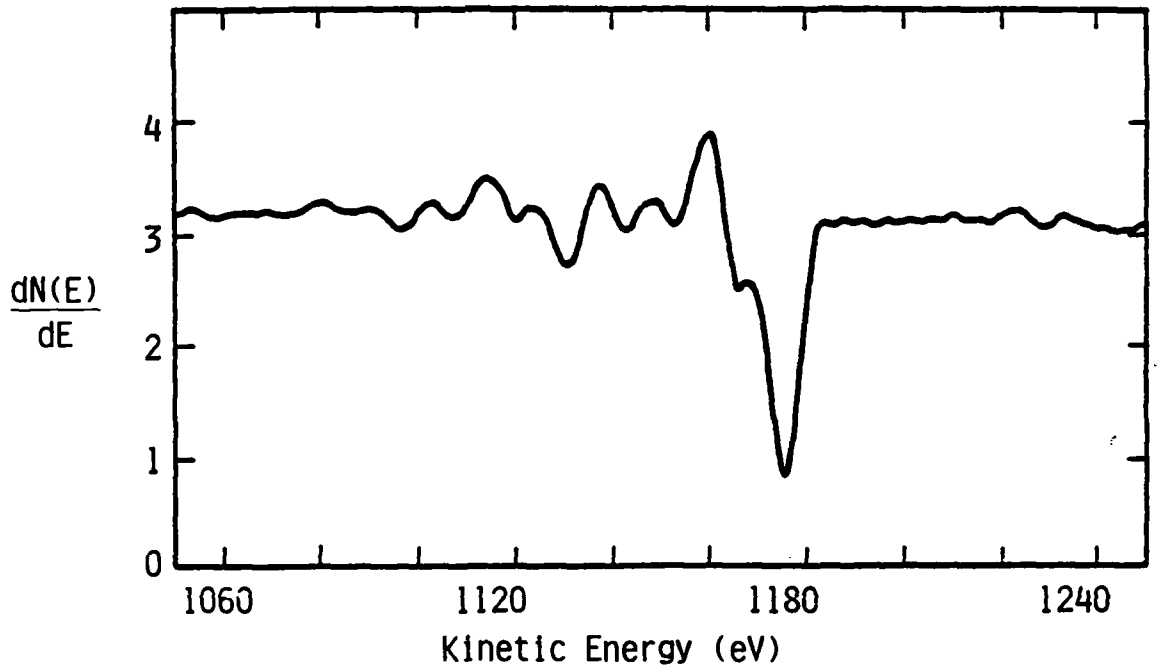

(e) Fiber surface in material held at 725°C for 30 minutes.

Figure 2 (continued). Expanded view of Mg peak in Auger electron spectra of fracture surfaces for all materials studied.

(a) As-received material.

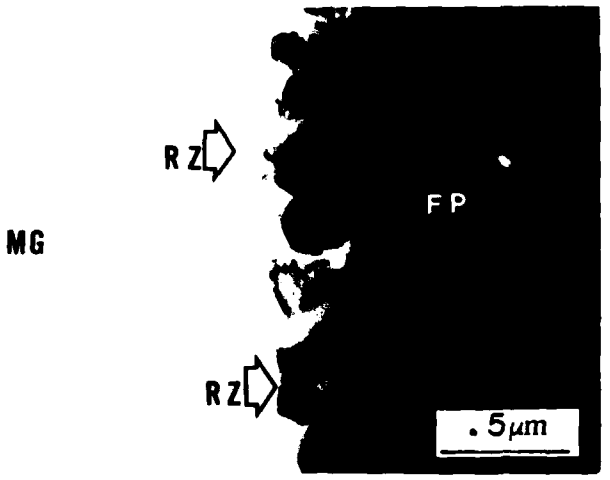

(b) Material held at 725°C for 15 minutes.

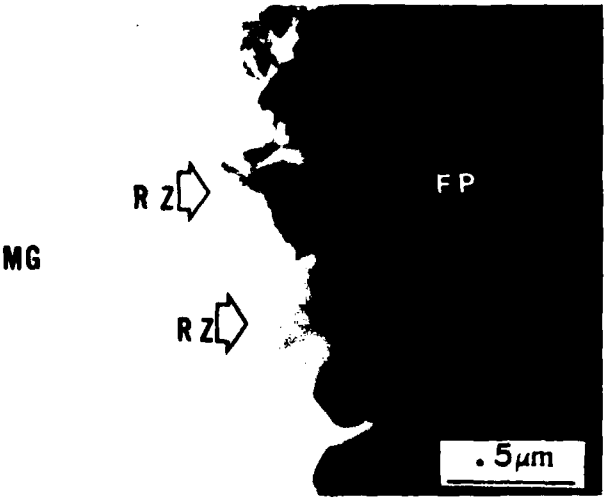

(c) Material held at 725°C for 15 minutes.

Figure 3. Transmission electron micrographs of fiber/matrix interfacial region in selected materials. The various constituents are indicated by: MG (C.P. Mg matrix); RZ (Reaction Zone product); and FP (Al_2O_3 fiber).

END

FILMED

8